

Generalization Bounds for Unsupervised Cross-Domain Mapping with WGANS

Tomer Galanti¹, Sagie Benaim¹, and Lior Wolf^{1,2}

¹School of Computer Science, Tel Aviv University

²Facebook AI Research

Abstract

The recent empirical success of cross-domain mapping algorithms, between two domains that share common characteristics, is not well-supported by theoretical justifications. This lacuna is especially troubling, given the clear ambiguity in such mappings. We work with the adversarial training method called the Wasserstein GAN. We derive a novel generalization bound, which limits the risk between the learned mapping h and the target mapping y , by a sum of two terms: (i) the risk between h and the most distant alternative mapping that was learned by the same cross-domain mapping algorithm, and (ii) the minimal Wasserstein GAN divergence between the target domain and the domain obtained by applying a hypothesis h^* on the samples of the source domain, where h^* is a hypothesis selected by the same algorithm. The bound is directly related to Occam’s razor and it encourages the selection of the minimal architecture that supports a small Wasserstein GAN divergence. From the bound, we derive algorithms for hyperparameter selection and early stopping in cross-domain mapping GANs. We also demonstrate a novel capability of estimating confidence in the mapping of every specific sample. Lastly, we show how non-minimal architectures can be effectively trained by an inverted knowledge distillation in which a minimal architecture is used to train a larger one, leading to higher quality outputs.

Keywords: Unsupervised learning, Cross-Domain Alignment, Adversarial Training, Wasserstein GANs

1. Introduction

The recent literature contains many examples of unsupervised learning that are beyond the classical work on clustering and density estimation, most of which revolve around generative models that are trained to capture a certain distribution. In many cases, the generation is unconditioned, and the learned hypothesis takes the form of $g(z)$ for a random vector z . It is obtained based on a training set containing i.i.d samples from the target domain.

The vast majority of the literature on this problem employs adversarial training, and specifically a variant of Generative Adversarial Networks (GANs), which were introduced by Goodfellow et al. (2014). GAN-based schemes typically employ two functions that are learned jointly: a generator g and a discriminator d . The discriminator is optimized to distinguish between “real” samples from the training set and “fake” samples that are generated as $g(z)$, where z is distributed according to a fixed known distribution. The generator is optimized to generate adversarial samples, i.e., samples $g(z)$, such that d would classify as real.

The ability to train a function $g(z)$ for a random z that captures the distribution underlying a given training set, is not surprising and there are suitable options, even without GANs. A simple example

would be sampling from the training set, which is unsatisfying due to the inability to generate novel samples. Other GAN-less options generate *de novo* samples, for example, various interpolation methods, including methods that fit noise (Bojanowski et al., 2017). The ability of GANs in generating samples from the target distribution was investigated theoretically by Arora et al. (2017).

Much less understood is the ability to learn, in a completely unsupervised manner, in the conditioned case, where the learned function g maps a sample from a source domain to the analogous sample in a target domain. First, it is unclear what analogous means, let alone to capture it in a formula. Second, as detailed in Sec. 2.2, the mapping problem is inherently ambiguous. While learning a conditional mapping, using a GAN was recently studied theoretically by Pan et al. (2018), we are unaware of such efforts in the unsupervised case.

Despite these theoretical challenges, the field of unsupervised cross-domain mapping, in which a sample from domain A is translated to a sample in domain B , is enjoying a great deal of empirical success, e.g, (Xia et al., 2016; Kim et al., 2017; Zhu et al., 2017; Yi et al., 2017; Benaim and Wolf, 2017; Liu et al., 2017a). We attribute this success to the simplicity hypothesis, meaning that these solutions learn the minimal complexity mapping, such that the discrepancy between the fitted distribution and the target distribution is small. As we show empirically, choosing the minimal complexity mapping eliminates the ambiguity of the problem.

In addition to the empirical validation, we present a generalization bound that supports the simplicity hypothesis. Bounding the error obtained with unsupervised methods is subject to an inherent challenge: without the ability to directly evaluate the risk on the training set, it is not clear on which grounds to build the bound. Specifically, typical generalization bounds of the form of training risk plus a regularization term cannot be used.

The bound we construct has a different form. As one component, it has the success of the fitting process. This is captured by the Wasserstein GAN (WGAN) (Arjovsky et al., 2017) divergence and is typically directly minimized by the learner. Another component is the maximal risk within the hypothesis class to any other hypothesis that also provides a good fit. This term is linked to minimal complexity, since it is expected to be small in minimal hypothesis classes, and it can be estimated empirically.

In addition to explaining the plausibility of unsupervised image to image mapping despite the inherent ambiguities, our analysis also directly leads to a set of new unsupervised cross domain mapping algorithms. By training pairs of networks that are distant from each other and both minimize the WGAN divergence, we are able to obtain a measure of confidence on the mapping’s outcome. This is surprising for two reasons: first, in the unsupervised settings, confidence estimation is almost unheard of, since it typically requires a second set of supervised samples. Second, confidence is hard to calibrate for multidimensional outputs. The confidence estimation holds both in expectation (Alg. 1), with application to hyperparameters selection (Alg. 2), and estimating per-sample loss (Alg. 3).

Another method that we derive based on our framework, is able to avoid the ambiguity of unsupervised mapping between domains, yet enjoy the expressiveness of deep neural networks. The method trains a pair of mappings that are close to each other (Alg. 4). The first mapping minimizes the WGAN divergence and has a minimal complexity. The second mapping, which is deeper, also minimizes the WGAN divergence, and in addition, is restricted to be close to the first network.

1.1 Relation to Our Previous Publications

The work described here is part of the line of work on the role of minimality in unsupervised learning that we have been following in conference publications (Galanti et al., 2018; Benaim et al., 2018). In this manuscript, we focus specifically on WGAN, while previous work employed a measure of discrepancy, and derive a precise generalization bound, which was missing in our previous work (the bounds of Benaim et al. (2018) are used for motivating the methods, but contain a term that cannot be estimated). The algorithms presented here, and the empirical results, are identical to those in the conference publications, except for Alg. 5, which is new.

2. Background

We briefly review IPMs, WGANs, the framework we use to define and then address the ambiguity in alignment, and previous work on the role of complexity in overcoming this ambiguity.

2.1 IPMs and WGANs

Integral Probability Metrics (or IPMs for short), first introduced by Müller (1997), is an important family of distance functions between distributions. For a given Polish space $\mathcal{S} = (\mathcal{X}, \|\cdot\|)$, two distributions D_1 and D_2 over \mathcal{X} and a class \mathcal{C} of functions $f : \mathcal{X} \rightarrow \mathbb{R}$, the \mathcal{C} -IPM between D_1 and D_2 is defined as follows:

$$\rho_{\mathcal{C}}(D_1, D_2) := \sup_{d \in \mathcal{C}} \left\{ \mathbb{E}_{x \sim D_1}[d(x)] - \mathbb{E}_{x \sim D_2}[d(x)] \right\} \quad (1)$$

This family of metrics includes a wide variety of GAN divergences, such as Arjovsky et al. (2017); Zhao et al. (2017); Berthelot et al. (2017); Li et al. (2015, 2017); Mroueh and Sercu (2017); Mroueh et al. (2018).

In this work we give special attention to the WGAN algorithm (Arjovsky et al., 2017) which inherits many features from IPMs. This is a variant of GAN, that uses the 1-Wasserstein distance instead of the original GAN divergence. The stability of WGAN was later improved by Gulrajani et al. (2017) and is currently one of the most successful ways to generate samples from a distribution defined by training samples. This algorithm aims to find a mapping g that takes a random sample from a noise distribution, D_z , and maps it into a random sample of D by minimizing the 1-Wasserstein distance between $g \circ D_z$ (the distribution of $g(z)$ for $z \sim D_z$) and D . For a given Polish space $\mathcal{S} = (\mathcal{X}, \|\cdot\|)$ and two distributions D_1 and D_2 over \mathcal{X} the 1-Wasserstein distance between two distributions D_1 and D_2 is defined as follows:

$$W(D_1, D_2) := \inf_{\gamma \in \mathcal{M}(D_1, D_2)} \mathbb{E}_{(x, y) \sim \gamma} [\|x - y\|] \quad (2)$$

Here, $\mathcal{M}(D_1, D_2)$ denotes the set of all joint distributions $\gamma(x, y)$, whose marginals are D_1 and D_2 (resp.). In general, computing the infimum in Eq. 2 is highly intractable. Nevertheless, by the Kantorovich-Rubinstein duality (cf. Villani (2003), Remark 6.5) we have the following equivalence:

$$W(D_1, D_2) = \sup_{\|d\|_{\text{Lip}} \leq 1} \left\{ \mathbb{E}_{x \sim D_1}[d(x)] - \mathbb{E}_{x \sim D_2}[d(x)] \right\} \quad (3)$$

where $d : \mathcal{X} \rightarrow \mathbb{R}$ is a 1-Lipschitz function and $\|d\|_{\text{Lip}} := \sup_{x, y \in \mathcal{X}} \frac{|d(x) - d(y)|}{\|x - y\|}$ is its Lipschitz norm. In order to employ the 1-Wasserstein distance for learning to generate samples from a target

distribution, Arjovsky et al. (2017) approximated $W(D_1, D_2)$ by implementing the members of $\mathcal{C} = \{d \mid \|d\|_{\text{Lip}} \leq 1\}$ using neural networks.

2.2 The Unsupervised Alignment Problem

In this paper, we consider the *Unsupervised Alignment Problem*. In this setting, there are two domains (\mathcal{X}_A, D_A) and (\mathcal{X}_B, D_B) where D_A and D_B are distributions over the sample spaces $\mathcal{X}_A \subset \mathbb{R}^N$ and $\mathcal{X}_B \subset \mathbb{R}^M$ respectively (we assume that the spaces are recruited with σ -algebras). In addition, there is a hypothesis class \mathcal{H} of functions $h : \mathcal{X}_A \rightarrow \mathbb{R}^M$ and a loss function $\ell : \mathbb{R}^M \times \mathbb{R}^M \rightarrow \mathbb{R}$. In this problem, the goal is to learn a mapping between the two domains $A = (\mathcal{X}_A, D_A)$ and $B = (\mathcal{X}_B, D_B)$ in an unsupervised manner with the only inputs are i.i.d samples from the two distributions D_A and D_B independently (all notations are listed in Appendix A, Tab. 1).

$$\mathcal{S}_A \xrightarrow{\text{i.i.d}} D_A^{m_1} \text{ and } \mathcal{S}_B \xrightarrow{\text{i.i.d}} D_B^{m_2} \quad (4)$$

We assume that there is a set \mathcal{T} of unknown target functions that map the first domain to the second domain, i.e., for every $y \in \mathcal{T}$, we have: $y : \mathcal{X}_A \rightarrow \mathcal{X}_B$ and $D_B = y \circ D_A$. The goal of the learning algorithm is to fit a function $h \in \mathcal{H}$ that is closest to some $y \in \mathcal{T}$,

$$h \in \arg \inf_{f \in \mathcal{H}} \left\{ \inf_{y \in \mathcal{T}} R_{D_A}[f, y] \right\} \quad (5)$$

Here, $R_D[f_1, f_2]$ is the generalization risk function between f_1 and f_2 for a distribution D , that is defined in the following manner:

$$R_D[f_1, f_2] := \mathbb{E}_{x \sim D} [\ell(f_1(x), f_2(x))] \quad (6)$$

In the unsupervised setting, one cannot estimate this risk on the training samples. Instead, the learner must rely on the two training sets $\{x_i\}_{i=1}^{m_1}$ and $\{y_j\}_{j=1}^{m_2}$. This, however, is inherently ambiguous, since for example, given an invertible mapping y , one cannot distinguish between this mapping and a mapping that replaces $y(x)$ by $y(\hat{x})$ for a pair of samples x, \hat{x} in the first domain such that $\mathbb{P}_{D_A}[x] = \mathbb{P}_{D_A}[\hat{x}]$, simply by observing the samples. This difficulty of recovering y and not one of the alternative functions \hat{y} such that $D_B = y \circ D_A = \hat{y} \circ D_A$ is termed in (Galanti et al., 2018) as “the alignment problem”. Note that since this ambiguity is independent to the size of the training set, and, is, in many ways, more fundamental than the estimation error that arises from limited training sets, we simply assume that the algorithm has full access to D_A and D_B themselves. Constructing the additional terms that reflect the estimation error is straightforward, e.g., using well-established statistical learning tools, such as the Radamacher complexity (Bartlett and Mendelson, 2003).

In the field of cross domain mapping, most contributions employ a circularity constraint (Xia et al., 2016; Kim et al., 2017; Zhu et al., 2017; Yi et al., 2017). Circularity requires the recovery of both y and y^{-1} simultaneously, using two hypotheses h and h' , respectively, with the following objective:

$$\inf_{h, h' \in \mathcal{H}} \text{GAN}_C(h \circ D_A, D_B) + \text{GAN}_C(h' \circ D_B, D_A) \quad (7a)$$

$$+ R_{D_A}[h' \circ h, \text{Id}_A] + R_{D_B}[h \circ h', \text{Id}_B] \quad (7b)$$

where $\text{GAN}_C(D_1, D_2)$ denotes the GAN divergence between distributions D_1 and D_2 that was first introduced by Goodfellow et al. (2014), defined as follows:

$$\text{GAN}_C(D_1, D_2) := \sup_{d \in \mathcal{C}} \left\{ \mathbb{E}_{x \sim D_1} [\log(1 - d(x))] + \mathbb{E}_{x \sim D_2} [\log(d(x))] \right\} \quad (8)$$

Here, \mathcal{C} is a set of discriminator functions. The terms in Eq. 7a ensure that the samples generated by mapping domain A to domain B follow the distribution of samples in domain B and vice versa. The terms in 7b are the circularity terms, which ensure that mapping a sample from one domain to the second and back, results in the original sample. Note that the first two terms match distributions (via the GAN scores) and the last two match individual samples (via the loss ℓ in the risk).

The circularity terms are shown empirically to improve the obtained results. However, these terms do not eliminate all of the inherent ambiguity. Let Π be an invertible permutation of the samples in domain B (*not* a permutation of the vector elements of the representation of samples in B). Galanti et al. (2018) explain that every circularity preserving pair h and h' gives rise to many alternative solutions of the form $\hat{h} = h \circ \Pi$ and $\hat{h}' = \Pi^{-1} \circ h'$

$$\begin{aligned} (h' \circ \Pi^{-1}) \circ (\Pi \circ h) &= h \circ h' \approx \text{Id}_A, \text{ and} \\ (\Pi \circ h) \circ (h' \circ \Pi^{-1}) &= \Pi \circ (h \circ h') \circ \Pi^{-1} \approx \Pi \circ \text{Id}_B \circ \Pi^{-1} = \text{Id}_B. \end{aligned} \quad (9)$$

If, in addition, Π satisfies $D_B(x) \approx D_B(\Pi(x))$, then the GAN terms of Eq. 7a are approximately invariant to this permutation.

Since both low GAN divergence and circularity cannot, separately or jointly, eliminate the ambiguity of the mapping problem, a complete explanation of the success of unsupervised cross-domain mapping must consider the hypothesis classes \mathcal{H} and \mathcal{C} . This is what we intend to do in Sec. 4.

3. The Simplicity Hypothesis

Despite the availability of a large number of alternative hypotheses h' that satisfy the constraints of Eq. 7, the methods of Xia et al. (2016); Kim et al. (2017); Zhu et al. (2017); Yi et al. (2017) enjoy empirical success, Why?

Our hypothesis is that *the small-discrepancy mappings of the lowest complexity approximate the alignment of the target functions*. We further hypothesize that when performing research in unsupervised mapping, goldilock architectures are selected. These architectures are complex enough to allow small discrepancies, but not complex enough to support mappings that are not minimal in complexity. By doing so, one of the minimal-complexity low-discrepancy mappings is learned.

3.1 An Illustrative Example

In order to illustrate our hypothesis, we present a very simple toy example, depicted in Fig. 1. Consider the domain A of uniformly distributed points $(x_1, x_2)^\top \in \mathbb{R}^2$, where $0 \leq x_1 < 1$ and $x_2 = 0.5$. Let B be a similar domain, except $x_2 = 2$. We are interested in learning the mapping $y_{AB}^{2D}((x_1, 0.5)^\top) = (x_1, 2)^\top$. We note that there are infinitely many mappings from domain A to B that satisfy the constraints of Eq. 7.

However, when we learn the mapping using a neural network with one hidden layer of size 2, and Leaky ReLU activations¹ (Maas et al., 2013), y_{AB}^{2D} is one of only two options. In this case $h(x) = \sigma_a(Wx + b)$, for $W \in \mathbb{R}^{2 \times 2}, b \in \mathbb{R}^2$ and where σ_a is applied per coordinate. The only admissible solutions are of the form $W_b = \begin{pmatrix} 1 & -2b_1 \\ 0 & 4 - 2b_2 \end{pmatrix}$ or $W'_b = \begin{pmatrix} -1 & 1 - 2b_1 \\ 0 & 4 - 2b_2 \end{pmatrix}$ and $b = (b_1, b_2)^\top$,

1. $\sigma_a(x) = \text{Ind}[x < 0]ax + \text{Ind}[x \geq 0]x$, for the indicator function $\text{Ind}[q]$ which maps a true value to one, zero otherwise.

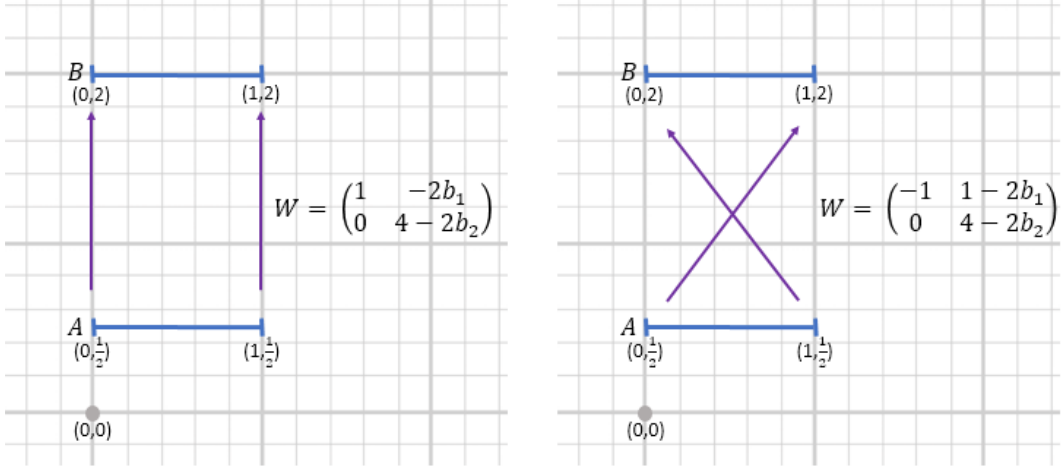


Figure 1: An illustrative example, where the two domains are line segments in \mathbb{R}^2 . There are infinitely many mappings that preserve the uniform distribution on the two segments. However, only two stand out as “semantic”. These are exactly the two mappings that can be captured by a neural network with only two hidden neurons and Leaky ReLU activations, i.e., by a function $h(x) = \sigma_a(Wx + b)$, for a weight matrix W and the bias vector b .

which are identical, for every b , to y_{AB}^{2D} or to an alternative $y_{AB}^{2D'}((x_1, 0.5)^\top) = (1 - x_1, 2)^\top$. Exactly the same situation holds for any pair of line segments in \mathbb{R}^d_+ .

Therefore, by restricting the hypothesis space of h , we eliminate all alternative solutions, except two. These two are exactly the two mappings that would commonly be considered “more semantic” than any other mapping, and can be expressed as the simplest possible mapping through a shared one dimensional space. While this is an extreme example, we believe that the principle is general, since limiting the complexity of the admissible solutions eliminates the solutions that are derived from a target function y by permuting the samples in the space \mathcal{X}_A , because such mixing requires added complexity.

4. Generalization Bounds for Cross Domain Mapping

In this section, we discuss sufficient conditions for overcoming the alignment problem. For simplicity, we first focus on the deterministic case, i.e., $\mathcal{T} = \{y\}$. The results are then extended, in Appendix B, to the non-deterministic case.

4.1 Terminology and Assumptions

Before we state our main results, we introduce some necessary terminology and assumptions. The real line is denoted by $\mathbb{R} := (-\infty, \infty)$ and the set of natural numbers by $\mathbb{N} := \{1, 2, \dots\}$. We denote by $\text{Id} : \mathcal{X} \rightarrow \mathcal{X}$ the identity function, i.e., for every $x \in \mathcal{X}_B$, $\text{Id}(x) = x$. For a vector $x = (x_1, \dots, x_m) \in \mathbb{R}^m$ we denote $\|x\|_2 := \sqrt{\sum_{i=1}^m x_i^2}$ the Euclidean norm of x and for a matrix $W \in \mathbb{R}^{m \times n}$, we denote by $\|W\|_2 := \max_{x \neq 0} \frac{\|Wx\|_2}{\|x\|_2}$ the induced operator norm of W . For a

differentiable function $f : \mathbb{R}^m \rightarrow \mathbb{R}^n$ and $x \in \mathbb{R}^m$, we denote by $\mathcal{J}_f(x) := \left(\frac{\partial f_i}{\partial \zeta_j}(x) \right)_{i \in [n], j \in [m]}$ the Jacobian matrix of f in x and for a twice differentiable function $f : \mathbb{R}^m \rightarrow \mathbb{R}$, we denote by $\mathbf{H}_f(x) := \left(\frac{\partial^2 f}{\partial \zeta_i \partial \zeta_j}(x) \right)_{i,j \in [m]}$ the Hessian matrix of f in x . For $f : \mathbb{R}^m \rightarrow \mathbb{R}$ we will use the gradient notation instead of the Jacobian notation, $\nabla f(x) = \mathcal{J}_f(x)$. Given a function $f : \mathcal{X}_1 \rightarrow \mathcal{X}_2$ (where $\mathcal{X}_1 \subset \mathbb{R}^m$ and $\mathcal{X}_2 \subset \mathbb{R}^n$), we denote $f \in C^r$ if f is r -times continuously differentiable and $f \in C_{\text{diff}}^r$ if $f \in C^r$, f is invertible and $f^{-1} \in C^r$. For a function $f : \mathbb{R}^m \rightarrow \mathbb{R}^n$ and $\mathcal{X} \subset \mathbb{R}^m$, we define, $\|F\|_{\infty, \mathcal{X}} := \sup_{x \in \mathcal{X}} \|f(x)\|_2$. In addition, given a function $f : \mathcal{X} \rightarrow \mathbb{R}^n$, we denote, $\|f\|_{\text{Lip}} = \sup_{x, y \in \mathcal{X}} \frac{\|f(x) - f(y)\|_2}{\|x - y\|_2}$ for a domain $\mathcal{X} \subset \mathbb{R}^m$. In particular, if \mathcal{X} is convex and f is differentiable, we have $\|f\|_{\text{Lip}} = \|\mathcal{J}_f\|_{\infty, \mathcal{X}}$. For a twice differentiable function $f : \mathcal{X} \rightarrow \mathbb{R}$ we denote $\beta(f) := \|\mathbf{H}_f\|_{\infty, \mathcal{X}}$. Given a set E and two functions $F : E \rightarrow \mathbb{R}$ and $G : E \rightarrow \mathbb{R}$, we denote, $\forall e \in E : F(e) \lesssim G(e)$ if and only if $\exists C > 0$ (independent of e) such that, $\forall e \in E : F(e) \leq C \cdot G(e)$. We consider a set of random (the randomness arises from the initializations, selection of the data, etc') cross domain mapping algorithms $\{\mathcal{A}_\omega\}_{\omega \in \Omega}$. Each algorithm \mathcal{A}_ω takes two distributions D_A and D_B (or $S_A \stackrel{\text{i.i.d.}}{\sim} D_A^{m_1}$ and $S_B \stackrel{\text{i.i.d.}}{\sim} D_B^{m_2}$ if it does not have full access to the two distributions) and returns a hypothesis $h \in \mathcal{H}$. Here, ω is the vector of hyperparameters of \mathcal{A}_ω and Ω is the set of all possible vectors of hyperparameters. We denote by \mathcal{P}_ω the set of possible outputs of \mathcal{A}_ω . This set is expected to be much sparser than \mathcal{H} .

Throughout the paper we assume that the sets $\mathcal{X}_A \subset \mathbb{R}^N$ and $\mathcal{X}_B \subset \mathbb{R}^M$ are convex and bounded. We also assume that $\mathcal{C} \subset C^2$ and that every function $f \in \mathcal{H} \cup \mathcal{T}$, such that $f : \mathcal{X}_A \rightarrow \mathcal{X}_B$ is measurable (with respect to the σ -algebras of \mathcal{X}_A and \mathcal{X}_B respectively). Our results are shown for the L_2 -loss (unless stated otherwise).

4.2 A Gentle Start

In this section, we provide insight and perspective on the main idea using a simple lemma from (Bennaim et al., 2018).

We consider the case where: $\Omega = \mathbb{N}$. In this case, we decompose the hypothesis class into complexity classes, $\mathcal{H} := \bigcup_{k=1}^{\infty} \mathcal{H}_k$ where $\mathcal{H}_k \subset \mathcal{H}_{k+1}$ for $k \in \mathbb{N}$. In addition, we denote by $C(h) := \arg \min_{k \in \mathbb{N}} [h \in \mathcal{H}_k]$ the complexity of $h \in \mathcal{H}$. Inspired by the WGAN algorithm (Arjovsky et al., 2017), we consider any algorithm \mathcal{A}_k that returns a generator from \mathcal{H}_k that has a small WGAN divergence, $\mathbf{W}(h \circ D_A, D_B) \leq \epsilon_0$. Here, $\epsilon_0 > 0$ is some fixed threshold. Therefore,

$$\mathcal{P}_k = \{h \in \mathcal{H}_k \mid \mathbf{W}(h \circ D_A, D_B) \leq \epsilon_0\} \quad (10)$$

In other words, similar to the way the ERM learning rule (Emprirical Risk Minimization) abstracts the specific details of the underlying algorithm, the abstraction of the WGAN algorithm that we consider in our analysis can be any algorithm that returns any hypothesis $h_1 \in \mathcal{P}_k$. The following lemma bounds the generalization risk of the learned hypothesis h_1 .

Lemma 1 *Assume the settings of Sec. 2.2 and Sec. 4. Then, for every function $h_1 \in \mathcal{P}_k$, we have:*

$$R_{D_A}[h_1, y] \lesssim \sup_{h_2 \in \mathcal{P}_k} R_{D_A}[h_1, h_2] + \inf_{h \in \mathcal{P}_k} R_{D_A}[h, y] \quad (11)$$

This lemma follows immediately from the triangle inequality (see Lem. 6 in Appendix C). It provides an upper bound on the generalization risk, $R_{D_A}[h_1, y]$, of the learned function, h_1 , which

is the argument that we would like to minimize. The upper bound is decomposed into two parts: $\sup_{h_2 \in \mathcal{P}_k} R_{D_A}[h_1, h_2]$ and $\inf_{h \in \mathcal{P}_k} R_{D_A}[h, y]$. The first term measures the maximal distance between h_1 and a different candidate $h_2 \in \mathcal{P}_k$. The second term is the approximation error of y in the class \mathcal{P}_k . By the definition of \mathcal{P}_k , we have: $\mathcal{P}_k \subset \mathcal{P}_{k+1}$. In particular, the bound leads to the following trade-off,

$$\begin{aligned} \sup_{h_2 \in \mathcal{P}_k} R_{D_A}[h_1, h_2] &\leq \sup_{h_2 \in \mathcal{P}_{k+1}} R_{D_A}[h_1, h_2] \\ \inf_{h \in \mathcal{P}_k} R_{D_A}[h, y] &\geq \inf_{h \in \mathcal{P}_{k+1}} R_{D_A}[h, y] \end{aligned} \quad (12)$$

Therefore, the first term is increasing with respect to k and the second term is decreasing with respect to k . We, therefore, advocate selecting the complexity $k \in \mathbb{N}$ that minimizes the diameter of \mathcal{P}_k , such that the approximation error is small.

We consider that for every $k \in \mathbb{N}$, the first term can be easily estimated by training $h_2 \in \mathcal{H}_k$ such that $\mathbf{W}(h_2 \circ D_A, D_B) \leq \epsilon_0$ and is maximally distant from h_1 . On the other hand, since the algorithm is not provided with paired matches $(x, y(x))$, it is not feasible to compute the second term. Therefore, this bound gives us very limited intuition on how to select \mathcal{H}_k , about the relationship between the two terms and their relationship with the WGAN divergence. In addition, it can be employed to estimate the generalization risk, only if we assume the second term is small as done in (Benaim et al., 2018). In Sec. 4.3, we provide generalization bounds that replace the second term with GAN-like divergences and capacity terms.

4.3 Generalization Bounds

The following theorem introduces a generalization bound for cross domain mapping with IPMs.

Theorem 1 (Cross-Domain Mapping with IPMs) *Assume the settings of Sec. 2.2 and Sec. 4. Let $\omega \in \Omega$, $h \in \mathcal{P}_\omega$ such that $h : \mathcal{X}_A \rightarrow \mathcal{X}_B$ and $d \in \mathcal{C}$ such that $\beta(d) \leq 1$. Then, for every $h_1 \in \mathcal{P}_\omega$, we have:*

$$R_{D_A}[h_1, y] \lesssim \sup_{h_2 \in \mathcal{P}_\omega} R_{D_A}[h_1, h_2] + \rho_{\mathcal{C}}(h \circ D_A, D_B) + \sqrt{R_{D_B}[h \circ y^{-1} - \text{Id}, \nabla d]} \quad (13)$$

Thm. 1 provides an upper bound on the generalization risk, $R_{D_A}[h_1, y]$, of a hypothesis h_1 that was selected by an algorithm \mathcal{A}_ω , which is the argument that we would like to minimize. First, we note that the upper bound can be rephrased as follows:

$$\sup_{h_2 \in \mathcal{P}_\omega} [h_1, h_2] + \inf_{h, d} \left\{ \rho_{\mathcal{C}}(h \circ D_A, D_B) + \sqrt{R_{D_B}[h \circ y^{-1} - \text{Id}, \nabla d]} \right\} \quad (14)$$

where the infimum is taken over $h \in \mathcal{P}_\omega$, such that, $h : \mathcal{X}_A \rightarrow \mathcal{X}_B$ and $d \in \mathcal{C}$, such that, $\beta(d) \leq 1$. This bound is decomposed into three parts: $\sup_{h_2 \in \mathcal{P}_\omega} [h_1, h_2]$, $\rho_{\mathcal{C}}(h \circ D_A, D_B)$ and $\sqrt{R_{D_B}[h \circ y^{-1} - \text{Id}, \nabla d]}$ (for arbitrary $h \in \mathcal{P}_\omega$ and $d \in \mathcal{C}$ such that $\beta(d) \leq 1$). The first term measures the maximal distance between h_1 and a different candidate h_2 from \mathcal{P}_ω . This term is small, whenever the set \mathcal{P}_ω is concentrated. The second and third terms behave as approximation error and capacity terms (resp.). The second term measures the value of the \mathcal{C} -IPM between $h \circ D_A$ and D_B of a hypothesis $h \in \mathcal{P}_\omega$. The third term measures the ability of a gradient ∇d to approximate the function $h \circ y^{-1} - \text{Id}$. In general, since we do not know the target function, y , we cannot estimate

this term. Nevertheless, this term can be treated as a capacity term and monotonically decreases, as \mathcal{C} is expanded. On the other hand, if \mathcal{C} is expanded, then, the second term increases.

Next, we present a generalization bound for cross-domain mapping with WGANs. In this case, we can get rid of the capacity term. This is desirable, since we cannot estimate this term. For this purpose, we define the following set:

$$\mathcal{Q} := \left\{ h : \mathcal{X}_A \rightarrow \mathcal{X}_B \mid \exists y \in \mathcal{T} : \|h \circ y^{-1} - \text{Id}\|_{\text{Lip}} \leq 1 \right\} \quad (15)$$

This set contains the functions $h \in \mathcal{H}$ that are weakly correlated with the target function y . By weakly correlated, we mean that their derivatives cannot be too far from each other. We note that this definition fits both the deterministic case and the non-deterministic case as well. In the deterministic case, the " $\exists y \in \mathcal{T}$ " is unnecessary.

The following corollary introduces a generalization bound for cross domain mapping with WGANs.

Corollary 2 (Cross-Domain Mapping with WGANs) *Assume the settings of Sec. 2.2 and Sec. 4. In addition, assume that $y \in C_{\text{diff}}^1$, $\mathcal{H} \subset C^1$ and that for every $\omega \in \Omega$, we have: $\mathcal{P}_\omega \cap \mathcal{Q} \neq \emptyset$. Then, for every $\omega \in \Omega$ and $h_1 \in \mathcal{P}_\omega$, we have:*

$$R_{D_A}[h_1, y] \lesssim \sup_{h_2 \in \mathcal{P}_\omega} R_{D_A}[h_1, h_2] + \inf_{h \in \mathcal{P}_\omega \cap \mathcal{Q}} \mathbf{W}(h \circ D_A, D_B) \quad (16)$$

Cor. 2 provides a simplified version of Thm. 1. This statement further assumes that y, y^{-1} and every $h \in \mathcal{H}$ are continuously differentiable. In addition, it is assumed that there is a function $h \in \mathcal{P}_\omega$ such that $\|h \circ y^{-1} - \text{Id}\|_{\text{Lip}} \leq 1$. In this case, the capacity term is eliminated and the \mathcal{C} -IPM is replaced with the WGAN divergence of h .

In order to motivate this last assumption, we consider the case where $M = N$. By Lem. 10 in Appendix C, the following is a stronger assumption: $\|h - y\|_{\text{Lip}} \leq \|y^{-1}\|_{\text{Lip}}^{-1}$. This stronger assumption holds if : (i) the Lipschitz constant of y^{-1} is small and (ii) there is a function $h \in \mathcal{P}_\omega$ such that that \mathcal{I}_h and \mathcal{I}_y are not too far from each other. The Lipschitz constant is commonly assumed to be bounded in image to image translation, for example in (Benaim and Wolf, 2017) employed for deriving an unsupervised image to image translation algorithm. Given that this constant is small, the approximation requirement between y and the function $h \in \mathcal{P}_\omega$ is not too restrictive.

4.4 The Relationship with the Simplicity Hypothesis

An important application of Cor. 2 arises, when working with the setting of Sec. 4.2 ($\Omega = \mathbb{N}$, $C(h)$, \mathcal{A}_k and \mathcal{P}_k stay the same, etc'). In this case, whenever $\mathcal{P}_k \cap \mathcal{Q} \neq \emptyset$, Cor. 16 is translated to:

$$R_{D_A}[h_1, y] \lesssim \sup_{h_2 \in \mathcal{P}_k} R_{D_A}[h_1, h_2] + \inf_{h \in \mathcal{P}_k \cap \mathcal{Q}} \mathbf{W}(h \circ D_A, D_B) \quad (17)$$

This upper bound is decomposed into two parts: $\sup_{h_2 \in \mathcal{P}_k} R_{D_A}[h_1, h_2]$ and $\inf_{h \in \mathcal{P}_k \cap \mathcal{Q}} \mathbf{W}(h \circ D_A, D_B)$. By the definition of \mathcal{P}_k , we have: $\mathcal{P}_k \subset \mathcal{P}_{k+1}$. In particular,

$$\begin{aligned} \sup_{h_2 \in \mathcal{P}_k} R_{D_A}[h_1, h_2] &\leq \sup_{h_2 \in \mathcal{P}_{k+1}} R_{D_A}[h_1, h_2] \\ \inf_{h \in \mathcal{P}_k \cap \mathcal{Q}} \mathbf{W}(h \circ D_A, D_B) &\geq \inf_{h \in \mathcal{P}_{k+1} \cap \mathcal{Q}} \mathbf{W}(h \circ D_A, D_B) \end{aligned} \quad (18)$$

Therefore, the first term is increasing with respect to k and the second term is decreasing with respect to k . Hence, we advocate *selecting the minimal complexity $k \in \mathbb{N}$ that minimizes the diameter of \mathcal{P}_k , such that the minimal WGAN divergence of a hypothesis in $\mathcal{P}_k \cap \mathcal{Q}$ is kept small*. In Sec. 5.1, we discuss the algorithmic aspects of estimating and minimizing the bound.

5. Consequences of the Bound

Cor. 2 leads to concrete predictions, which are verified in Sec. 6. The first one states that in contrast to the current common wisdom, one can learn a semantically aligned mapping between two spaces without any matching samples and even without circularity.

Prediction 1 *When learning with a small enough network in an unsupervised way a mapping between domains that share common characteristics, the GAN constraint in the target domain is sufficient to obtain a semantically aligned mapping.*

The strongest clue that helps identify the alignment of the semantic mapping from the other mappings, is the suitable complexity of the network that is learned. A network with a complexity that is too low cannot replicate the target distribution, when taking inputs in the source domain (high discrepancy). A network that has a complexity that is too high, would not learn the minimal complexity mapping, since it could be distracted by other alignment solutions.

We believe that the success of the recent methods results from selecting the architecture used in an appropriate way. For example, DiscoGAN (Kim et al., 2017) employs either eight or ten layers, depending on the dataset. We make the following prediction:

Prediction 2 *When learning in an unsupervised way a mapping between domains, the complexity of the network needs to be carefully adjusted.*

This prediction is also surprising, since in supervised learning, extra depth is not as detrimental, if at all. As far as we know, this is the first time that this clear distinction between supervised and unsupervised learning is made².

5.1 Estimating the Ground Truth Error

Eq. 17 along with Eq. 10, provide us with an accessible upper bound for the generalization risk:

$$R_{D_A}[h_1, y] \lesssim \sup_{h_2 \in \mathcal{P}_k} R_{D_A}[h_1, h_2] + \epsilon_0 \quad (19)$$

Hence, for any fixed $k \in \mathbb{N}$, the right hand side can be directly approximated by training a neural network $h_2 \in \mathcal{H}_k$ that has a discrepancy at most ϵ_0 (i.e., $h_2 \in \mathcal{P}_k$) and has the maximal risk with regards to h_1 , i.e.,

$$\sup_{h_2 \in \mathcal{H}_k} R_{D_A}[h_1, h_2] \text{ s.t. } \mathbf{W}(h_2 \circ D_A, D_B) \leq \epsilon_0 \quad (20)$$

It is computationally impossible to compute the solution h_2 to Eq. 20, since, in most cases we cannot explicitly compute the set \mathcal{P}_k . Therefore, inspired by Lagrange relaxation, we employ the following

2. The MDL literature was developed when, people believed that small hypothesis classes are desired for both supervised and unsupervised learning.

Algorithm 1 Deciding when to stop training h_1

Require: S_A and S_B : unlabeled training sets; \mathcal{H} : a hypothesis class; ϵ_0 : a threshold; k : a complexity value; λ : a trade-off parameter; T_1 : a fixed number of epochs for h_1 ; T_2 : a fixed number of epochs for h_2 .

- 1: Initialize $h_1^0 \in \mathcal{H}_k$ and $h_2^0 \in \mathcal{H}_k$ at random.
- 2: **for** $t = 1, \dots, T_1$ **do**
- 3: Train $h_1^{t-1} \in \mathcal{H}_k$ for one epoch to minimize $W(h_1^t \circ D_A, D_B)$, obtaining $h_1^t \in \mathcal{H}_k$.
- 4: Train $h_2^{t-1} \in \mathcal{H}_k$ for T_2 epochs to minimize $W(h_2^t \circ D_A, D_B) - \lambda R_{D_A}[h_1^t, h_2^t]$, obtaining $h_2^t \in \mathcal{H}_k$.
 $\triangleright T_2$ provides a fixed comparison point.
- 5: **end for**
- 6: **return** h_1^t such that: $t = \arg \min_{i \in [T_1]} \left\{ R_{D_A}[h_1^i, h_2^i] \mid \forall j = 1, 2 : W(h_j^t \circ D_A, D_B) \leq \epsilon_0 \right\}$.

relaxed version of Eq. 20:

$$\min_{h_2 \in \mathcal{H}_k} \left\{ W(h_2 \circ D_A, D_B) - \lambda R_{D_A}[h_1, h_2] \right\} \quad (21)$$

where $\lambda > 0$ is a trade-off parameter. The expectation over $x \sim D_A$ (resp $x \sim D_B$) in the risk and discrepancy are replaced, as is often done, with the sum over the training samples in domain A (resp B). Based on this, we present a stopping criterion in Alg. 1. Eq. 21 is manifested in Step 6 (last line) as the selection criterion.

5.2 Deriving an Unsupervised Variant of Hyperband using the Bound

In order to optimize multiple hyperparameters simultaneously, we create an unsupervised variant of the hyperband method Li et al. (2016). Hyperband requires the evaluation of the loss for every configuration of hyperparameters. In our case, our loss is the risk function, $R_{D_A}[h_1, y]$. Since we cannot compute the actual risk, we replace it with an approximated value of our bound

$$\sup_{h_2 \in \mathcal{P}_\omega} R_{D_A}[h_1, h_2] + W(h_1 \circ D_A, D_B) \quad (22)$$

This expression differs from the original bound, since instead of having $\inf_{h \in \mathcal{P}_\omega \cap \mathcal{Q}} W(h \circ D_A, D_B)$ we replace it with $W(h_1 \circ D_A, D_B)$ which can be easily estimated. This term can fit as a good replacement, whenever $\inf_{h \in \mathcal{P}_\omega \cap \mathcal{Q}} W(h \circ D_A, D_B) \approx \inf_{h \in \mathcal{P}_\omega} W(h \circ D_A, D_B)$ since $\inf_{h \in \mathcal{P}_\omega} W(h \circ D_A, D_B) \leq W(h_1 \circ D_A, D_B)$. In addition, we choose \mathcal{A}_ω to be the WGAN algorithm, where ω is a set of hyperparameters that includes: the complexity of the trained network, batch size, learning rate, etc'.

In particular, the function ‘run_then_return_val_loss’ in the hyperband algorithm (Alg. 1 of Li et al. (2016)), which is a plug-in function for loss evaluation, is provided with our bound from Eq. 22 after training h_2 , as in Eq. 21. Our variant of this function is listed in Alg. 2. It employs two additional procedures that are used to store the learned models h_1 and h_2 at a certain point in the training process and to retrieve these to continue the training for a large amount of epochs. The retrieval function is simply a map between a vector of hyperparameters and a tuple of the learned networks and the number of epochs T when stored. For a new vector of hyperparameters, it returns $T = 0$

Algorithm 2 Unsupervised run_then_return_val_loss for hyperband

Require: S_A and S_B : unlabeled training sets; λ : a trade-off parameter; T : number of epochs. ω : set of hyperparameters.

- 1: $[h_1, h_2, T_{\text{last}}] = \text{return_stored_functions}(\omega)$
- 2: Train $h_1 \in \mathcal{H}_k$ for $T - T_{\text{last}}$ epochs to minimize $\mathbf{W}(h_1 \circ D_A, D_B)$.
- 3: Train $h_2 \in \mathcal{H}_k$ for $T - T_{\text{last}}$ epochs to minimize $\mathbf{W}(h_2 \circ D_A, D_B) - \lambda R_{D_A}[h_1, h_2]$.
- 4: $\text{store_functions}(\omega, [h_1, h_2, T])$
- 5: **return** $R_{D_A}[h_1, h_2] + \mathbf{W}(h_1 \circ D_A, D_B)$.

Algorithm 3 Bounding the loss of h_1 on sample x

Require: S_A and S_B : unlabeled training sets; \mathcal{H} : a hypothesis class; $h_1 \in \mathcal{H}$: a mapping; λ : a trade-off parameter; x : a specific sample.

- 1: Train $h_2 \in \mathcal{H}$ to minimize $\mathbf{W}(h_2 \circ D_A^x, D_B) - \lambda \ell(h_1(x), h_2(x))$.
- 2: **return** $\ell(h_1(x), h_2(x))$.

and two randomly initialized networks, with architectures that are determined by the given set of hyperparameters. When a network is retrieved, it is then trained for a number of epochs that is the difference between the required number of epochs T , which is given by the hyperband method, and the number of epochs it was already trained, denoted by T_{last} .

5.3 Bound on the Loss of Each Sample

Next, we extend the bound to estimate the error $\ell(h_1(x), y(x))$ of mapping by h_1 a specific sample $x \sim D_A$. Lem. 3 gives rise to a simple method for bounding the loss of h_1 on a specific sample $x \sim D_A$. Note that the second term in the bound does not depend on h_1 and is expected to be small, since it denotes the capability of overfitting on a single sample x .

Lemma 3 *Let $A = (X_A, D_A)$ and $B = (X_B, D_B)$ be two domains and \mathcal{P} a class of functions. In addition, let ℓ be a loss function satisfying the triangle inequality. Then, for any target function y and $h_1 \in \mathcal{P}$, we have:*

$$\ell(h_1(x), y(x)) \leq \sup_{h_2 \in \mathcal{P}} \ell(h_1(x), h_2(x)) + \inf_{h \in \mathcal{P}} \ell(h(x), y(x)) \quad (23)$$

Similar to the analysis done in Sec. 5.1, Eq. 23 provides us with an accessible bound for the per-sample loss. In this case, we take $\mathcal{P} = \{h \in \mathcal{H} \mid \mathbf{W}(h \circ D_A^x, D_B) \leq \epsilon_0\}$, where D_A^x is the distribution of $s = x$ with probability 0.5 and $s \sim D_A$ with probability 0.5. This reweighting emphasizes the role of x and allows us to train h_2 for fewer epochs. This is important, since, different h_2 must be trained for measuring the error of each sample x . The RHS can be directly approximated by training a neural network h_2 of a discrepancy lower than ϵ and has maximal loss with regards to h_1 , i.e.,

$$\sup_{h_2 \in \mathcal{H}} \ell(h_1(x), h_2(x)) \text{ s.t. } \mathbf{W}(h_2 \circ D_A^x, D_B) \leq \epsilon_0 \quad (24)$$

With similar considerations as in Sec. 5.1, we replace Eq. 24 with the following objective:

$$\min_{h_2 \in \mathcal{H}} \mathbf{W}(h_2 \circ D_A^x, D_B) - \lambda \ell(h_1(x), h_2(x)) \quad (25)$$

As before, the expectation over $x \sim D_A$ and $x \sim D_B$ in the discrepancy, are replaced with the sum over the training samples in domain A and B (resp.).

5.4 Alignment with Non-minimal Architectures

If the simplicity hypothesis is correct, then in order to capture the target alignment, one would need to learn with the minimal complexity architecture that supports a small discrepancy. However, complex architectures can lead to even smaller discrepancies and to better outcomes.

In order to enjoy both the alignment provided by our hypothesis and the improved output quality, we propose to find a function h of a non-minimal complexity k_2 that minimizes the following objective function

$$\min_{h \text{ s.t. } C(h)=k_2} \left\{ W(h \circ D_A, D_B) + \lambda \inf_{g \text{ s.t. } C(g)=k_1} R_{D_A}[h, g] \right\} \quad (26)$$

where k_1 is the minimal complexity for mapping with low discrepancy between domain A and domain B . In other words, we suggest to find a function h that is both a high complexity mapping from domain A to B and is close to a function of low complexity. The term $\inf_{g \text{ s.t. } C(g)=k_1} R_{D_A}[h, g]$ is

a regularization term that restricts the function h to be aligned with a function of smaller complexity. There are alternative ways to implement an algorithm that minimizes the objective function presented in Eq. 26. Assuming, based on this equation, that for h that minimizes the objective function, the corresponding $g^* = \inf_{g \text{ s.t. } C(g)=k_1} R_{D_A}[h, g]$ has a (relatively) small discrepancy, leads to a two-step algorithm. The algorithm first finds a function g that has small complexity and small discrepancy and then finds h of a larger complexity that is close to g . This is implemented in Alg. 4. Note that in the first step, k_1 is being estimated, for example, by gradually increasing its value, until g with a discrepancy lower than a threshold ϵ_0 is found. We suggest using a liberal threshold, since the goal of the network g is to provide alignment and not the lowest possible discrepancy.

Algorithm 4 Complexity Based Regularization Alignment

Require: S_A and S_B : unlabeled training sets; k_2 : a desired complexity; ϵ_0 : a threshold; λ : a trade-off parameter.

- 1: Identify the minimal complexity k_1 , which leads to a small discrepancy $k_1 = \arg \min_{k \in \mathbb{N}} \left\{ \min_{g \text{ s.t. } C(g)=k} W(g \circ D_A, D_B) \leq \epsilon_0 \right\}$.
- 2: Train g of complexity k_1 to minimize $W(g \circ D_A, D_B)$.
- 3: Train h of complexity k_2 to minimize $W(h \circ D_A, D_B) + \lambda R_{D_A}[h, g]$.

6. Experiments

The first group of experiments is intended to test the validity of the two predictions made, in order to give further support to the simplicity hypothesis. The next group of experiments are dedicated to testing Algs. 1, 2 and 3. Finally, we evaluate the success of Alg. 4 in comparison to the DiscoGAN method of Kim et al. (2017) (additional experiments validating Alg. 5 from Appendix B are presented there).

Note that while we develop the theoretical results in the context of IPMs and WGAN, the methods developed are widely applicable. In order to demonstrate this, we run our experiments using a large

variety of GAN variants, including CycleGAN Zhu et al. (2017), DiscoGAN Kim et al. (2017), DistanceGAN Benaim and Wolf (2017), and UNIT Liu et al. (2017b), as well as using WGAN itself. The choice of relying on WGAN in the analysis was made, since it is highly accepted as an effective GAN method and since it is amenable to analysis.

6.1 Experiments for the Predictions

Prediction 1 states that since the unsupervised mapping methods are aimed at learning minimal complexity low discrepancy functions, GANs are sufficient. In this paper, we mainly focus on a complexity measure that is the minimal number of layers of a neural network that are required in order to compute h , where each hidden layer is of size $\in [r_1, r_2]$. In the literature (Zhu et al., 2017; Kim et al., 2017), learning a mapping $h : \mathcal{X}_A \rightarrow \mathcal{X}_B$, based only on the GAN constraint on B , is presented as a failing baseline. In (Yi et al., 2017), among many non-semantic mappings obtained by the GAN baseline, one can find images of GANs that are successful. However, this goes unnoticed. In order to validate the prediction that a purely GAN based solution is viable, we conducted a series of experiments using the DiscoGAN architecture and GAN loss in the target distribution only. We consider image domains A and B , where $\mathcal{X}_A = \mathcal{X}_B = \mathbb{R}^{3 \times 64 \times 64}$.

In DiscoGAN, the generator is built of: (i) an encoder consisting of convolutional layers with 4×4 filters, followed by Leaky ReLU activation units and (ii) a decoder consisting of deconvolutional layers with 4×4 filters, followed by a ReLU activation units. Sigmoid is used for the output layer. Between four to five convolutional/deconvolutional layers are used, depending on the domains used in A and B (we match the published code architecture per dataset). The discriminator is similar to the encoder, but has an additional convolutional layer as the first layer and a sigmoid output unit.

The first set of experiments considers the CelebA face dataset. Transformations are learned between the subset of images labeled as male and those labeled as female, as well as from blond to black hair. The results are shown in Fig. 2 and 3 (resp.). It is evident that the output image is closely related to the input images, despite the fact that cycle loss terms were not used.

In the case of mapping handbags to shoes, as seen in Fig. 4, the GAN does not provide a meaningful solution. However, in the case of edges to shoes and vice versa (Fig. 5), the GAN solution is successful.

In Prediction 2, we predict that the selection of the right number of layers is crucial in unsupervised learning. Using fewer layers than needed, will not support the modeling of the target distribution. By contrast, adding superfluous layers would mean that more and more alternative mappings obscure the target transformation.

In (Kim et al., 2017), 8 or 10 layers are employed (counting both convolution and deconvolution) depending on the experiment. In our experiment, we vary the number of layers and inspect the influence on the results. The experiments are also repeated for the Wasserstein GAN loss (using the same architecture, except, for the generator, the last sigmoid layer is removed).

These experiments were done on the CelebA gender conversion task, where 8 layers are employed in the experiments of (Kim et al., 2017). Using the public implementation and adding and removing layers, we obtain the results in Figs. 6–11 for WGAN and Figs. 12–15 for DiscoGAN. Note that since the encoder and the decoder parts of the learned network are symmetrical, the number of layers is always even. As can be seen, changing the number of layers has a dramatic effect on the results. For the WGAN case, the best overall results are obtained at 6 layers. Using fewer layers, WGAN often fails to produce images of the desired class. Adding layers, the semantic alignment is lost, as

expected. For the DiscoGAN case, the best results are obtained at 6 or 8 layers with 6 having the best alignment and 8 having better discrepancy. The results degrade quickly, as one deviates from the optimal value. Using fewer layers, the GAN fails to produce images of the desired class. Adding layers, the semantic alignment is lost, just as expected.

Additional experiment was conducted in order to verify that these conclusions extend to the CycleGAN architecture of Zhu et al. (2017). The results are shown in Fig. 16. As can be seen, running an experiment on the Aerial images to Maps dataset, we found that 8 layers produce an aligned solution. Using 10 layers produces unaligned map images with low discrepancy. For fewer than 8 layer, the discrepancy is high and the images are not very detailed.

Note that Kim et al. (2017) have preferred low discrepancy over alignment in their choice. In other words, the selected architecture of size $k = 8$ presents acceptable images at the price of lower alignment compared to an architecture of size $k - 2$. This is probably a result of ambiguity that is already present at the size k architecture. On the other hand, the smaller architecture of size $k - 2$ does not produce images of extremely low discrepancy, and there is no architecture that benefits both, an extremely low discrepancy and high alignment. This is observed, for example in Fig. 12, where females are translated to males. For 4 layers the discrepancy is too low and the mapping fails to produce images of males. For 6 layers, the discrepancy is relatively low and the alignment is at its highest. For 8 layers, the discrepancy is at its lowest value. Nevertheless, the alignment is worse.

6.2 Results for Algs. 1 and 2

We test the two algorithms on two unsupervised alignment methods: DiscoGAN (Kim et al., 2017) and DistanceGAN (Benaim and Wolf, 2017). In DiscoGAN, we train h_1 (and h_2), using two GANs and two circularity constraints; in DistanceGAN, one GAN and one distance correlation loss are used. The published parameters for each dataset are used, except when applying our model selection method, where we vary the number of layers and when using hyperband, where we also vary the learning rate and the batch size.

Five datasets were used in the experiments: (i) aerial photographs to maps, trained on data scraped from Google Maps (Isola et al., 2017), (ii) the mapping between photographs from the cityscapes dataset and their per-pixel semantic labels (Cordts et al., 2016), (iii) architectural photographs to their labels from the CMP Facades dataset (Radim Tyleček, 2013), (iv) handbag images Zhu et al. (2016) to their binary edge images as obtained from the HED edge detector (Xie and Tu, 2015), and (v) a similar dataset for the shoe images from (Yu and Grauman, 2014).

Throughout the experiments, fixed values are used as the low-discrepancy threshold ($\epsilon_0 = 0.2$). The tradeoff parameter between the dissimilarity term and the fitting term during the training of h_2 is set, per dataset, to be the maximal value, such that the fitting of h_2 provides a solution that has a discrepancy lower than the threshold, $W(h_2 \circ D_A, D_B) \leq \epsilon_0$. This is done once, for the default parameters of h_1 , as given in the original DiscoGAN and DistanceGAN Kim et al. (2017); Benaim and Wolf (2017).

The results of all experiments are summarized in Tab. 3, which presents the correlation and p-value between the ground truth error, as a function of the independent variable, and the bound. The independent variable is either the training epoch or the sample, depending on the algorithm tested. For example, in Alg. 1 we wish to decide on the best epoch, the independent variable is the training epoch. A high correlation (low p-value) between the bound and the ground truth error, both as a function of the number of layers, indicates the validity of the bound and the utility of the algorithm.

Similar correlations are shown with the GAN losses and the reconstruction losses (DiscoGAN) or the distance correlation loss (DistanceGAN), in order to demonstrate that these are much less correlated with the ground truth error. In the plots of Fig. 17, we omit the other scores in order to reduce clutter.

Stopping Criterion (Alg. 1) For testing the stopping criterion suggested in Alg. 1, we compared, at each time point, two scores that are averaged over all training samples: $\|h_1(x) - h_2(x)\|$, which is our bound in Eq. 19 (excluding the $+\epsilon_0$ term), and the ground truth error $\|h_1(x) - y(x)\|$, where $y(x)$ is the ground truth image that matches x in domain B .

Note that similar to the experiments with ground truth in the literature Kim et al. (2017); Zhu et al. (2017); Benaim and Wolf (2017), the ground truth error is measured in the label space and not in the image domain. The mapping in the other direction y is not one to one.

The results are depicted in the main results table (Tab. 3) as well as in Fig. 17 for both DiscoGAN (first column) and DistanceGAN (second column). As can be seen, there is an excellent match between the mean ground truth error of the learned mapping h_1 and the predicted error. No such level of correlation is present when considering the GAN losses or the reconstruction losses (for DiscoGAN), or the distance correlation loss of DistanceGAN. Specifically, the very low p-values in the first column of Tab. 3 show that there is a clear correlation between the ground truth error and our bound for all datasets. For the other columns, the values in question are chosen to be the losses used for h_1 . The lower scores in these columns show that none of these values are as correlated with the ground truth error, and so cannot be used to estimate this error.

In the experiment of Alg. 1 for DiscoGAN, which has a large number of sample points, the cycle from B to A and back to B is significantly correlated with the ground truth error with very low p-values in four out of five datasets. However, its correlation is significantly lower than that of our bound.

In Fig. 17, the Facades graph shows a different behavior than the other graphs. This is because the Facades dataset is inherently ambiguous and presents multiple possible mappings from A to B . Each mapping satisfies the Occam’s razor property separately.

Selecting Architecture with the Modified Hyperband Algorithm Our bound is used in Sec. 5.2 to create an unsupervised variant of the hyperband method. In addition to selecting the architecture, this allows for the optimization of multiple hyperparameters at once, while enjoying the efficient search strategy of the hyperband method.

Fig. 19 demonstrates the applicability of our unsupervised hyperband-based method for different datasets, employing both DiscoGAN and DistanceGAN. The graphs show the error and the bound obtained for the selected configuration after up to 35 hyperband iterations. As can be seen, in all cases, the method is able to recover a configuration that is significantly better than what is recovered, when only optimizing for the number of layers. To further demonstrate the generality of our method, we applied it on the UNIT Liu et al. (2017b) architecture. Specifically, for DiscoGAN and DistanceGAN we optimize the number of encoder and decoder layer, batch size and learning rate, while for UNIT, we optimize for the number of encoder and decoder layers, number of resnet layers and learning rate. Fig. 18 and Tab. 19(b) show the convergence on the hyperband method.

Predicting per-Sample loss with Alg. 3 Finally, we consider the per sample loss. The results are reported numerically in Tab. 3 and plotted in Figs. 20– 22. As can be seen, there is a high degree of correlation between the measured bound and the ground truth error. Therefore, our method is able to reliably predict the per-sample success of a multivariate mapping learned in a fully unsupervised manner.

This correlation also seems to hold when considering the time axis, i.e., we can combine Alg. 1 and Alg. 3 and select the stopping epoch that is best for a specific sample. The results are shown in Fig. 23.

6.3 Results for Alg. 4

The goal of Alg. 4 is to find a well-aligned solution with higher complexity than the minimal solution and potentially smaller discrepancy. It has two stages. In the first one, k_1 , which is the minimal complexity that leads to a low discrepancy, is identified. This follows a set of experiments that are similar to the one that is captured, for example, by Fig. 2. To demonstrate robustness, we select a single value of k_1 across all experiments. Specifically, we use $k_1 = 6$, which, as discussed above, typically leads to a low (but not very low) discrepancy, while the alignment is still unambiguous.

Once g is trained, we proceed to the next step of optimizing a second network of complexity k_2 . Note that while the first function (g) uses the complete DiscoGAN architecture, the second network (h) only employs a one-directional mapping, since alignment is obtained by g . Figs. 24–29 depict the obtained results, for a varying number of layers. First, the result obtained by the DiscoGAN method with k_1 is displayed. The results of applying Alg. 4 are then displayed for a varying k_2 .

As can be seen, our algorithm leads to more sophisticated mappings. Kim et al. (2017) have noted that their solutions are, at many times, related to texture or style transfer and, for example, geometric transformations are not well-captured. The new method is able to better capture such complex transformations. Consider the case of mapping male to female in Fig. 24, first row. A man with a beard is mapped to a female image. While for g the beard is still somewhat present, it is not so for h with $k_2 > k_1$. On the female to male mappings in Fig. 25, it is evident in most mappings that g produces a more blurred image, while h is more coherent for $k_2 > k_1$. Another example is in the blond to black hair mapping in Fig. 25. In the 5th row, the style transfer nature of g is evident, since it maps a red object behind the head together with the whole blond hair, producing an unrealistic black hair. The h of complexity $k_2 = 8$ is able to separate that object from the hair, and in $k_2 > 8$ it produces realistic looking black hair. This kind of transformation requires more than a simple style transfer. On the edges to shoes and edges to handbags mappings of Fig. 28 and Fig. 29, while the general structure is clearly present, it is significantly sharpened by mapping h with $k_2 > k_1$.

For the face datasets, we also employ face descriptors in order to learn whether the mapping is semantic. We can check if the identity is preserved post mapping, by comparing the VGG face descriptors of Parkhi et al. (2015). One can assume that two matching images that match will have many similar features and so the VGG representation will be similar. The cosine similarities are used, as is commonly done.

In addition, we train a linear classifier in the space of the VGG face descriptors, in order to distinguish between Male/Female, Eyeglasses/No-eyeglasses, and Blond/Black. This allows us to check, beyond discrepancy, that the mapping indeed transforms between the domains. The training samples in domains A and B are used to train this classifier, which is then applied to a set of test images before and after mapping, measuring the accuracy. The higher the accuracy, the better the separation.

Tab. 2 presents the results for both the k_1 layers network g , alternative networks g of higher complexity (shown as baseline only), and the network h trained using Alg. 4. We expect the alignment of g to be best at complexity k_1 , and worse due to the loss of discrepancy for alternative network g with complexity $k > k_1$. We expect this loss of alignment to be resolved for networks h trained with Alg. 4.

In the experiments of black to blond hair and blond to black hair mappings, we note that h with $k_2 = 8$ has the best descriptor similarity, and very good separation accuracy and discrepancy. Higher values of k_2 are best in terms of separation accuracy and discrepancy, but lose somewhat in descriptor similarity. A similar situation occurs for male to female and female to male mappings and in eyeglasses to non-eyeglasses, where $k_2 = 8$ results in the best similarity score and higher values of k_2 result in better separation accuracy and discrepancy.

It is interesting to note, that the distance between g and h is also minimal for $k_2 = 8$. Perhaps, with more effective optimization, higher complexities could also maintain similarity, while delivering lower discrepancies.

7. Conclusions

The recent success in mapping between two domains in an unsupervised way and without any existing knowledge, other than network hyperparameters, is nothing less than extraordinary and has far reaching consequences. As far as we know, nothing in the existing machine learning or cognitive science literature suggests that this would be possible.

We provide an intuitive definition of function complexity and employ it in order to identify minimal complexity mappings, which we show to play a pivotal role in this success. If our hypothesis is correct, simply by training networks that are not too complex, the target mapping stands out from all other alternative mappings.

Our analysis leads directly to a new unsupervised cross domain mapping algorithm that is able to avoid the ambiguity of such mapping, yet enjoy the expressiveness of deep neural networks. These methods are based on training a pair of mappings that are close to each other.

By training pairs of networks that are distant from each other, we are able to obtain a confidence measure on the mapping’s outcome. The confidence estimation holds both in expectation, with application to hyperparameter selection, and per sample, thus supporting dynamic confidence-based run time behavior, and (future work) unsupervised boosting during training.

In Sec. 4, we derived a novel generalization bound for the unsupervised learning of mappings between domains. While one can argue that the term “generalization bound” does not apply, since there is no training error to be generalized, we believe that the term is appropriate: first, the various terms on the right hand side can be matched to the conventional terms of measured error and a capacity term. Second, during training, we learn a function, even if in an unsupervised manner, and we are interested in estimating its distance from the target function on unseen (“test”) samples.

The new bound does not address the estimation error that arises from employing finite sets of samples. Terms to capture this error can be readily inserted by employing conventional techniques, such as Rademacher Complexity, PAC-Bayes, VC-Theory, etc’. Needless to say, those techniques cannot be applied here without our results, due to the inability to estimate the training error.

Acknowledgements

This project has received funding from the European Research Council (ERC) under the European Union’s Horizon 2020 research and innovation programme (grant ERC CoG 725974).

References

Martín Arjovsky, Soumith Chintala, and Léon Bottou. Wasserstein generative adversarial networks. In *Proceedings of the 34th International Conference on Machine Learning, ICML 2017*, pages 214–223, 2017.

Sanjeev Arora, Rong Ge, Yingyu Liang, Tengyu Ma, and Yi Zhang. Generalization and equilibrium in generative adversarial nets (gans). In *Proceedings of the 34th International Conference on Machine Learning, ICML 2017, Sydney, NSW, Australia, 6-11 August 2017*, pages 224–232, 2017. URL <http://proceedings.mlr.press/v70/arora17a.html>.

Peter L. Bartlett and Shahar Mendelson. Rademacher and gaussian complexities: Risk bounds and structural results. *J. Mach. Learn. Res.*, 3:463–482, March 2003.

Sagie Benaim and Lior Wolf. One-sided unsupervised domain mapping. In *Advances in Neural Information Processing Systems*, pages 752–762, 2017.

Sagie Benaim, Tomer Galanti, and Lior Wolf. Estimating the success of unsupervised image to image translation. In *ECCV*, 2018.

David Berthelot, Tom Schumm, and Luke Metz. Began: Boundary equilibrium generative adversarial networks. *CoRR*, 2017.

Piotr Bojanowski, Armand Joulin, David Lopez-Paz, and Arthur Szlam. Optimizing the latent space of generative networks. *arXiv preprint arXiv:1707.05776*, 2017.

Marius Cordts, Mohamed Omran, Sebastian Ramos, Timo Rehfeld, Markus Enzweiler, Rodrigo Benenson, Uwe Franke, Stefan Roth, and Bernt Schiele. The cityscapes dataset for semantic urban scene understanding. In *CVPR*, 2016.

Tomer Galanti, Lior Wolf, and Sagie Benaim. The role of minimal complexity functions in unsupervised learning of semantic mappings. *International Conference on Learning Representations*, 2018.

Ian Goodfellow, Jean Pouget-Abadie, Mehdi Mirza, Bing Xu, David Warde-Farley, Sherjil Ozair, Aaron Courville, and Yoshua Bengio. Generative adversarial nets. In *NIPS*, pages 2672–2680. 2014.

Ishaan Gulrajani, Faruk Ahmed, Martin Arjovsky, Vincent Dumoulin, and Aaron C Courville. Improved training of wasserstein gans. In I. Guyon, U. V. Luxburg, S. Bengio, H. Wallach, R. Fergus, S. Vishwanathan, and R. Garnett, editors, *Advances in Neural Information Processing Systems 30*, pages 5767–5777. Curran Associates, Inc., 2017.

Phillip Isola, Jun-Yan Zhu, Tinghui Zhou, and Alexei A Efros. Image-to-image translation with conditional adversarial networks. In *CVPR*, 2017.

Taeksoo Kim, Moonsu Cha, Hyunsoo Kim, Jungkwon Lee, and Jiwon Kim. Learning to discover cross-domain relations with generative adversarial networks. *arXiv preprint arXiv:1703.05192*, 2017.

Chun-Liang Li, Wei-Cheng Chang, Yu Cheng, Yiming Yang, and Barnabas Poczos. Mmd gan: Towards deeper understanding of moment matching network. In I. Guyon, U. V. Luxburg, S. Bengio, H. Wallach, R. Fergus, S. Vishwanathan, and R. Garnett, editors, *Advances in Neural Information Processing Systems 30*, pages 2203–2213. Curran Associates, Inc., 2017.

Lisha Li, Kevin G. Jamieson, Giulia DeSalvo, Afshin Rostamizadeh, and Ameet Talwalkar. Efficient hyperparameter optimization and infinitely many armed bandits. *arXiv preprint arXiv:1603.06560*, 2016.

Yujia Li, Kevin Swersky, and Richard Zemel. Generative moment matching networks. In *Proceedings of the 32Nd International Conference on International Conference on Machine Learning - Volume 37*, ICML’15, pages 1718–1727. JMLR, 2015.

Ming-Yu Liu, Thomas Breuel, and Jan Kautz. Unsupervised image-to-image translation networks. In *Advances in Neural Information Processing Systems*, pages 700–708, 2017a.

Ming-Yu Liu, Thomas Breuel, and Jan Kautz. Unsupervised image-to-image translation networks. In *NIPS*. 2017b.

Andrew L Maas, Awni Y Hannun, and Andrew Y Ng. Rectifier nonlinearities improve neural network acoustic models. In *in ICML Workshop on Deep Learning for Audio, Speech and Language Processing*, 2013.

Youssef Mroueh and Tom Sercu. Fisher GAN. In *Advances in Neural Information Processing Systems 30: Annual Conference on Neural Information Processing Systems 2017, 4-9 December 2017, Long Beach, CA, USA*, pages 2510–2520, 2017.

Youssef Mroueh, Chun-Liang Li, Tom Sercu, Anant Raj, and Yu Cheng. Sobolev GAN. In *International Conference on Learning Representations*, 2018.

Alfred Müller. Integral probability metrics and their generating classes of functions advances in applied probability. In *Advances in Applied Probability*, pages 429—443, 1997.

Xudong Pan, Mi Zhang, and Daizong Ding. Theoretical analysis of image-to-image translation with adversarial learning. In Jennifer Dy and Andreas Krause, editors, *Proceedings of the 35th International Conference on Machine Learning*, volume 80 of *Proceedings of Machine Learning Research*, pages 4003–4012, Stockholm Sweden, 10–15 Jul 2018. PMLR.

O. M. Parkhi, A. Vedaldi, and A. Zisserman. Deep face recognition. In *British Machine Vision Conference*, 2015.

Radim Šára Radim Tyleček. Spatial pattern templates for recognition of objects with regular structure. In *Proc. GCPR*, 2013.

Sathamangalam Ranga Iyengar Srinivasa Varadhan. Lecture notes on limit theorems, 2002.

C. Villani. *Topics in Optimal Transportation*. Graduate studies in mathematics. American Mathematical Society, 2003.

Yingce Xia, Di He, Tao Qin, Liwei Wang, Nenghai Yu, Tie-Yan Liu, and Wei-Ying Ma. Dual learning for machine translation. *arXiv preprint arXiv:1611.00179*, 2016.

Saining Xie and Zhuowen Tu. Holistically-nested edge detection. In *ICCV*, 2015.

Zili Yi, Hao Zhang, Ping Tan, and Minglun Gong. Dualgan: Unsupervised dual learning for image-to-image translation. *arXiv preprint arXiv:1704.02510*, 2017.

A. Yu and K. Grauman. Fine-grained visual comparisons with local learning. In *CVPR*, 2014.

Junbo Jake Zhao, Michaël Mathieu, and Yann LeCun. Energy-based generative adversarial network. In *International Conference on Learning Representations (ICLR)*, 2017.

Jun-Yan Zhu, Philipp Krähenbühl, Eli Shechtman, and Alexei A. Efros. Generative visual manipulation on the natural image manifold. In *ECCV*, 2016.

Jun-Yan Zhu, Taesung Park, Phillip Isola, and Alexei A Efros. Unpaired image-to-image translation using cycle-consistent adversarial networkss. *arXiv preprint arXiv:1703.10593*, 2017.

Appendix A. Summary of Notations

Table 1: Summary of Notation

ℓ	A loss function, in this paper, we mostly use the L_2 loss
\mathbb{P}, \mathbb{E}	The probability and expectation symbols
\mathbb{R}, \mathbb{N}	The real line and the set of natural numbers
A, B	Two domains $A = (X_A, D_A)$ and $B = (X_B, D_B)$
$R_D[f_1, f_2]$	The generalization risk between f_1 and f_2 w.r.t distribution D (see Eq. 6)
\mathcal{H}, h	A hypothesis class and a specific hypothesis
\mathcal{C}, d	A set of discriminators and a specific discriminator
\mathcal{T}, y	A set of target functions and a target function
$\mathcal{M}(D_1, D_2)$	The set of all joint distributions $\gamma(x, y)$, whose marginals are D_1 and D_2 (resp.)
$\text{GAN}_{\mathcal{C}}(D_1, D_2)$	The GAN divergence between the distributions D_1 and D_2 (see Eq. 8)
$\rho_{\mathcal{C}}(D_1, D_2)$	The \mathcal{C} -IPM divergence between D_1 and D_2 (see Eq. 1)
$\mathbf{W}(D_1, D_2)$	The 1-Wasserstein distance between D_1 and D_2 (see Eqs. 2 and 3)
Ω, ω	A set of vectors of hyperparamers and a specific vector of hyper-parameters
\mathcal{A}_{ω}	A cross-domain mapping algorithm with hyperparameters ω
\mathcal{P}_{ω}	The set of possible outputs of \mathcal{A}_{ω}
$C(h)$	The complexity of a hypothesis $h \in \mathcal{H}$
\mathcal{H}_k	A hypothesis class of functions of complexity $\leq k$
\mathcal{A}_k	A cross-domain mapping algorithm of generators from \mathcal{H}_k
\mathcal{P}_k	The set of possible outputs of \mathcal{A}_k (see Eq. 10)
$\ x\ _2$	The Euclidean norm of a vector x
$\ X\ _2$	The induced operator norm of a matrix X
$\ f\ _{\text{Lip}}$	The Lipschitz norm of f
$\nabla f(x)$	The gradient of $f : \mathbb{R}^M \rightarrow \mathbb{R}$ in x
$\mathcal{J}_f(x)$	The Jacobian matrix of $f : \mathbb{R}^m \rightarrow \mathbb{R}^n$ in x
$\mathbf{H}_f(x)$	The Hessian matrix of $f : \mathbb{R}^m \rightarrow \mathbb{R}$ in x
$\beta(f)$	The maximal norm of the Hessian of $f : \mathbb{R}^m \rightarrow \mathbb{R}$
Id	The identity function
C^r	The set of r -times continuously differentiable functions
C_{diff}^r	The set of invertible functions f , such that $f, f^{-1} \in C^r$
Q	A set of functions that are restricted to be weakly correlated with a target function (see Eq. 15)

Appendix B. A Generalization Bound for the Non-Deterministic Case

In this section, we extend the discussion in Sec. 4 to the non-deterministic case. Our notion of non-determinism assumes that there are multiple target functions from A to B , i.e., $|\mathcal{T}| > 1$.

B.1 Generalization Bounds

The following theorem extends Thm. 1 to the non-deterministic case.

Theorem 2 (Cross-Domain Mapping with IPMs - The Non-Deterministic Case) *Assume the settings of Sec. 2.2 and Sec. 4. Let $\omega \in \Omega$, $h \in \mathcal{P}_\omega$ such that $h : \mathcal{X}_A \rightarrow \mathcal{X}_B$ and $d \in \mathcal{C}$ such that $\beta(d) \leq 1$. Then, for every $h_1 \in \mathcal{P}_\omega$, we have:*

$$\inf_{y \in \mathcal{T}} R_{D_A}[h_1, y] \lesssim \sup_{h_2 \in \mathcal{P}_\omega} R_{D_A}[h_1, h_2] + \rho_C(h \circ D_A, D_B) + \inf_{y \in \mathcal{T}} \sqrt{R_{D_B}[h \circ y^{-1} - \text{Id}, \nabla d]} \quad (27)$$

The difference between Thm. 1 and Thm. 2 is intuitive: in the latter, the theorem bounds the term, $\inf_{y \in \mathcal{T}} R_{D_A}[h_1, y]$, instead of the term $R_{D_A}[h_1, y]$ in the deterministic case. In addition, the capacity term in the deterministic case is replaced with its infimum with respect to $y \in \mathcal{T}$.

The following corollary extends Cor. 2. It introduces a generalization bound for cross domain mapping with WGANs for the non-deterministic case.

Corollary 4 (Cross-Domain Mapping with WGANs - The Non-Deterministic Case) *Assume the settings of Sec. 2.2 and Sec. 4. In addition, assume that $\mathcal{T} \in C_{\text{diff}}^1$, $\mathcal{H} \subset C^1$ and that for every $\omega \in \Omega$, we have: $\mathcal{P}_\omega \cap \mathcal{Q} \neq \emptyset$. Then, for every $\omega \in \Omega$ and $h_1 \in \mathcal{P}_\omega$, we have:*

$$\inf_{y \in \mathcal{T}} R_{D_A}[h_1, y] \lesssim \sup_{h_2 \in \mathcal{P}_\omega} R_{D_A}[h_1, h_2] + \inf_{h \in \mathcal{P}_\omega \cap \mathcal{Q}} W(h \circ D_A, D_B) \quad (28)$$

The bound is decomposed into two parts: $\sup_{h_2 \in \mathcal{P}_\omega} R_{D_A}[h_1, h_2]$ and $\inf_{h \in \mathcal{P}_\omega \cap \mathcal{Q}} W(h \circ D_A, D_B)$. Since there are multiple possible target functions $y \in \mathcal{T}$ and $\sup_{h_2 \in \mathcal{P}_\omega} R_{D_A}[h_1, h_2]$ is almost the diameter of \mathcal{P}_ω , this term can be large, if $h_1 \approx y_1$ and $h_2 \approx y_2$, where $y_1, y_2 \in \mathcal{T}$ such that $y_1 \neq y_2$.

A tighter bound would result, if we are able to focus on the relevant y for each $h \in \mathcal{P}_\omega$. In order to concentrate the different functions in \mathcal{P}_ω around the same target function, we minimize the bound with respect to ω . This way, we are able to select ω that concentrates the members of \mathcal{P}_ω around the same target function. In other words, we select ω that minimizes the diameter of \mathcal{P}_ω such that the 1-Wasserstein distances of the hypotheses in \mathcal{P}_ω are kept small. In Sec. B.2.1, we extend the algorithmic aspects of estimating and minimizing the bound in the non-deterministic case.

B.2 Equivalence Classes According to a Fixed Encoder

We assume that by fixing the first layers of the mapping y , this ambiguity vanishes, and only one possible solution remains, e.g., in a common case where the learned hypothesis is viewed as an encoder followed by a decoder, that the function is determined by the encoder part.

In this case, the hypothesis class $\mathcal{H} := \{h_{\theta, \omega} = g_\theta \circ f_\omega \mid \theta \in \Theta, \omega \in \Omega\}$ consists of hypotheses that are parameterized by two sets of parameters $\theta \in \Theta$ and $\omega \in \Omega$. In addition, we denote $\mathcal{H}_\omega := \{h_{\theta, \omega} \mid \theta \in \Theta\}$. Specifically, \mathcal{H} serves as a set of neural networks of a fixed architecture

with $l_1 + l_2$ layers. Each hypothesis $h_{\theta, \omega}$ is a neural network of an encoder-decoder architecture. The encoder, f_ω , consists of the first l_1 layers and the decoder, g_θ , consists of the last l_2 layers. In addition, ω and θ denote the sets of weights of f_ω and g_θ (resp.).

We take \mathcal{A}_ω that returns a generator from \mathcal{H}_ω that has small WGAN divergence $\mathbf{W}(h \circ D_A, D_B) \leq \epsilon_0$ for some fixed threshold $\epsilon_0 > 0$. In this case, we have: $\mathcal{P}_\omega := \{h \in \mathcal{H}_\omega \mid \mathbf{W}(h \circ D_A, D_B) \leq \epsilon_0\}$.

B.2.1 ESTIMATING THE GROUND TRUTH ERROR

Cor. 4 provides us with an accessible upper bound for the generalization risk of the learned function h_1 . In general, for every $\omega \in \Omega$, we can approximate $\sup_{h_2 \in \mathcal{P}_\omega} [h_1, h_2]$ simply by maximizing $R_{D_A}[h_1, h_2]$ with respect to $h_2 \in \mathcal{P}_\omega$. On the other hand, in order to approximate the second term, we can simply minimize $\mathbf{W}(h \circ D_A, D_B)$ for $h \in \mathcal{P}_\omega$. This can only give a heuristic approximation for the second term, since we do not suffice that $h \in \mathcal{Q}$. Therefore, instead of computing the bound in Eq. 28, we use the following approximate version of it:

$$\sup_{h_2 \in \mathcal{P}_\omega} R_{D_A}[h_1, h_2] + \mathbf{W}(h_1 \circ D_A, D_B) \quad (29)$$

Thus, for any fixed $\omega \in \Omega$, the first term in the RHS can be directly approximated by training a neural network $h_2 \in \mathcal{H}_\omega$ that has a WGAN divergence lower than ϵ_0 and has the maximal risk, with regards to h_1 , i.e.,

$$\sup_{h_2 \in \mathcal{H}_\omega} R_{D_A}[h_1, h_2] \text{ s.t. } \mathbf{W}(h_2 \circ D_A, D_B) \leq \epsilon_0 \quad (30)$$

It is computationally impossible to compute the solution h_2 to Eq. 30, since in most cases we cannot explicitly compute the set \mathcal{P}_ω . Therefore, inspired by Lagrange relaxation, we employ the following relaxed version of Eq. 30:

$$\min_{h_2 \in \mathcal{H}_\omega} \left\{ \mathbf{W}(h_2 \circ D_A, D_B) - \lambda R_{D_A}[h_1, h_2] \right\} \quad (31)$$

The expectation over $x \sim D_A$ (resp $x \sim D_B$) in the risk and discrepancy are replaced, as is often done, with the sum over the training samples in domain A (resp B). Based on this, we present a stopping criterion in Alg. 5. Eq. 31 is manifested in Step 6.

B.2.2 EXPERIMENTAL RESULTS FOR ALG. 5

For testing the stopping criterion suggested in Alg. 5, we plotted the value of the bound and attached a specific sample for a few epochs. For this purpose, we employed DiscoGAN for both h_1 and h_2 , such that the encoder part is shared between them. As we can see in Figs. 30–31, for smaller values of the bound, we obtain more realistic images and the alignment also improves.

Algorithm 5 Deciding when to stop training h_1

Require: S_A and S_B : unlabeled training sets; \mathcal{H} : a hypothesis class; ϵ_0 : a threshold; λ : a trade-off parameter; T_0 : a fixed number of epochs for ω ; T_1 : a fixed number of epochs for h_1 ; T_2 : a fixed number of epochs for h_2 .

- 1: Initialize $\omega_0 \in \Omega$ at random.
- 2: Initialize $\theta_{1,0}, \theta_{2,0} \in \Theta$ at random.
- 3: **for** $t = 1, \dots, T_0$ **do**
- 4: Train ω_{t-1} for one epoch to minimize $R_{D_A}[h_1^{t-1}, h_2^{t-1}] + W(h_1^{t-1} \circ D_A, D_B)$, obtaining $\omega_t \in \Omega$.
- 5: Train $\theta_{1,t-1} \in \Theta$ for T_1 epochs to minimize $W(h_1^t \circ D_A, D_B)$, obtaining $\theta_{1,t} \in \Theta$.
- 6: Train $\theta_{2,t-1} \in \Theta$ for T_2 epochs to minimize $W(h_2^t \circ D_A, D_B) - \lambda R_{D_A}[h_1^t, h_2^t]$, obtaining $\theta_{2,t} \in \Theta$.
- 7: ▷ Here, $h_i^t := g_{\theta_{i,t-1}} \circ f_{\omega_{t-1}}$ for $i = 1, 2$.
- 8: Define $t := \arg \min_{i \in [T_0]} \left\{ R_{D_A}[h_1^i, h_2^i] + W(h_1^i \circ D_A, D_B) \mid \forall j = 1, 2 : W(h_j^t \circ D_A, D_B) \leq \epsilon_0 \right\}$.
- 9: **return** h_1^t .

Appendix C. Proofs of Thm. 1 and Cor. 2

The following lemma bounds the generalization risk between a hypothesis h and a target function y . The upper bound is a function of the \mathcal{C} -IPM between the distributions $h \circ D_A$ and D_B . An additional term expresses the approximation of $h(x) - y(x)$ by the gradient of a function $d \in \mathcal{C}$. Both terms are multiplied by a term that depends on the smoothness of d .

Lemma 5 *Assume the settings of Sec. 2.2 and Sec. 4. Let $y \in \mathcal{T}$ be target function and $d \in \mathcal{C}$ such that $\beta(d) < 2$. Then, for every function $h \in \mathcal{H}$, such that $h : \mathcal{X}_A \rightarrow \mathcal{X}_B$, we have:*

$$R_{D_A}[h, y] \leq \frac{2\rho_C(h \circ D_A, D_B)}{2 - \beta(d)} + \frac{2 \sup_{u \in \mathcal{X}_A} \|h(u) - y(u)\|_2}{2 - \beta(d)} \sqrt{R_{D_B}[h \circ y^{-1} - \text{Id}, \nabla d]} \quad (32)$$

Proof First, since each function $f \in \mathcal{H} \cup \mathcal{T}$, such that $f : \mathcal{X}_A \rightarrow \mathcal{X}_B$, is measurable, by a change of variables (cf. Varadhan (2002), Thm. 1.9), we can represent the \mathcal{C} -IPM in the following manner:

$$\begin{aligned} \rho_C(h \circ D_A, D_B) &= \sup_{d \in \mathcal{C}} \left\{ \mathbb{E}_{u \sim h \circ D_A}[d(u)] - \mathbb{E}_{v \sim D_B}[d(v)] \right\} \\ &= \sup_{d \in \mathcal{C}} \left\{ \mathbb{E}_{u \sim h \circ D_A}[d(u)] - \mathbb{E}_{v \sim y \circ D_A}[d(v)] \right\} \\ &= \sup_{d \in \mathcal{C}} \left\{ \mathbb{E}_{x \sim D_A}[d \circ h(x)] - \mathbb{E}_{x \sim D_A}[d \circ y(x)] \right\} \\ &= \sup_{d \in \mathcal{C}} \left\{ \mathbb{E}_{x \sim D_A}[d \circ h(x) - d \circ y(x)] \right\} \end{aligned} \quad (33)$$

For fixed $d \in \mathcal{C}$ and $z \in \mathcal{X}_B$, we can write the following Taylor series:

$$d(z + \delta) - d(z) = \langle \nabla d(z), \delta \rangle + \frac{1}{2} \langle \delta^\top \cdot H_d(u^*), \delta \rangle \quad (34)$$

where u^* is strictly between z and $z + \delta$ (on the line connecting z and $z + \delta$). In particular, for each $d \in \mathcal{C}$ and $x \in \mathcal{X}_A$, if $z = y(x)$ and $\delta = h(x) - y(x)$, we have:

$$\begin{aligned} d(h(x)) - d(y(x)) &= \langle \nabla_{y(x)} d(y(x)), h(x) - y(x) \rangle \\ &\quad + \frac{1}{2} \left\langle (h(x) - y(x))^{\top} \cdot \mathbf{H}_d(u_{d,x}^*), h(x) - y(x) \right\rangle \end{aligned} \quad (35)$$

where $u_{d,x}^*$ is strictly between $y(x)$ and $h(x)$ (on the line connecting $y(x)$ and $h(x)$). Therefore, by combining Eqs. 33 and 35, we obtain that for every $d \in \mathcal{C}$, we have:

$$\begin{aligned} \rho_{\mathcal{C}}(h \circ D_A, D_B) &\geq \mathbb{E}_{x \sim D_A} [d(h(x)) - d(y(x))] \\ &= \mathbb{E}_{x \sim D_A} \left[\langle \nabla_{y(x)} d(y(x)), h(x) - y(x) \rangle \right] \\ &\quad + \frac{1}{2} \mathbb{E}_{x \sim D_A} \left[\left\langle (h(x) - y(x))^{\top} \cdot \mathbf{H}_d(u_{d,x}^*), (h(x) - y(x)) \right\rangle \right] \\ &= \mathbb{E}_{x \sim D_A} \left[\|h(x) - y(x)\|_2^2 \right] \\ &\quad + \mathbb{E}_{x \sim D_A} \left[\langle \nabla_{y(x)} d(y(x)) - (h(x) - y(x)), h(x) - y(x) \rangle \right] \\ &\quad + \frac{1}{2} \mathbb{E}_{x \sim D_A} \left[\left\langle (h(x) - y(x))^{\top} \cdot \mathbf{H}_d(u_{d,x}^*), h(x) - y(x) \right\rangle \right] \end{aligned} \quad (36)$$

In particular, by $|\mathbb{E}[X]| \leq \mathbb{E}[|X|]$, we have:

$$\begin{aligned} \rho_{\mathcal{C}}(h \circ D_A, D_B) &\geq \mathbb{E}_{x \sim D_A} \left[\|h(x) - y(x)\|_2^2 \right] - \left| \mathbb{E}_{x \sim D_A} \left[\langle \nabla_{y(x)} d(y(x)) - (h(x) - y(x)), h(x) - y(x) \rangle \right] \right| \\ &\quad - \frac{1}{2} \left| \mathbb{E}_{x \sim D_A} \left[\left\langle (h(x) - y(x))^{\top} \cdot \mathbf{H}_d(u_{d,x}^*), h(x) - y(x) \right\rangle \right] \right| \\ &\geq \mathbb{E}_{x \sim D_A} \left[\|h(x) - y(x)\|_2^2 \right] - \mathbb{E}_{x \sim D_A} \left[\left| \langle \nabla_{y(x)} d(y(x)) - (h(x) - y(x)), h(x) - y(x) \rangle \right| \right] \quad (37) \\ &\quad - \frac{1}{2} \mathbb{E}_{x \sim D_A} \left[\left| \left\langle (h(x) - y(x))^{\top} \cdot \mathbf{H}_d(u_{d,x}^*), h(x) - y(x) \right\rangle \right| \right] \end{aligned}$$

By applying the Cauchy-Schwartz inequality,

$$\begin{aligned} &\left| \langle \nabla_{y(x)} d(y(x)) - (h(x) - y(x)), h(x) - y(x) \rangle \right| \\ &\leq \|\nabla_{y(x)} d(y(x)) - (h(x) - y(x))\|_2 \cdot \|h(x) - y(x)\|_2 \\ &\leq \|\nabla_{y(x)} d(y(x)) - (h(x) - y(x))\|_2 \cdot \sup_{u \in \mathcal{X}_A} \|h(u) - y(u)\|_2 \end{aligned} \quad (38)$$

Again, by applying the Cauchy-Schwartz inequality,

$$\begin{aligned} \left| \left\langle (h(x) - y(x))^{\top} \cdot \mathbf{H}_d(u_{d,x}^*), h(x) - y(x) \right\rangle \right| &\leq \|(h(x) - y(x))^{\top} \cdot \mathbf{H}_d(u_{d,x}^*)\|_2 \cdot \|h(x) - y(x)\|_2 \\ &\leq \|\mathbf{H}_d(u_{d,x}^*)\|_2 \cdot \|h(x) - y(x)\|_2^2 \end{aligned} \quad (39)$$

Since \mathcal{X}_B is convex, $y(x), h(x) \in \mathcal{X}_B$ and $u_{d,x}^*$ is on the line connecting $y(x)$ and $h(x)$, we have: $u_{d,x}^* \in \mathcal{X}_B$. In particular,

$$\begin{aligned} \left| \left\langle (h(x) - y(x))^{\top} \cdot \mathbf{H}_d(u_{d,x}^*), h(x) - y(x) \right\rangle \right| &\leq \sup_{z \in \mathcal{X}_B} \|\mathbf{H}_d(z)\|_2 \cdot \|h(x) - y(x)\|_2^2 \\ &= \beta(d) \cdot \|h(x) - y(x)\|_2^2 \end{aligned} \quad (40)$$

Therefore, by combining Eqs. 37, 38 and 40, we have:

$$\begin{aligned}
 \rho_C(h \circ D_A, D_B) &\geq \mathbb{E}_{x \sim D_A} [||h(x) - y(x)||_2^2] - \frac{1}{2} \mathbb{E}_{x \sim D_A} [\beta(d) \cdot ||h(x) - y(x)||_2^2] \\
 &\quad - \sup_{u \in \mathcal{X}_A} ||h(u) - y(u)||_2 \cdot \mathbb{E}_{x \sim D_A} [||\nabla_{y(x)} d(y(x)) - (h(x) - y(x))||_2] \\
 &= \left(1 - \frac{\beta(d)}{2}\right) R_{D_A}[h, y] \\
 &\quad - \sup_{u \in \mathcal{X}_A} ||h(u) - y(u)||_2 \cdot \mathbb{E}_{x \sim D_A} [||\nabla_{y(x)} d(y(x)) - (h(x) - y(x))||_2]
 \end{aligned} \tag{41}$$

By Jensen's inequality,

$$\mathbb{E}_{x \sim D_A} [||\nabla_{y(x)} d(y(x)) - (h(x) - y(x))||_2] \leq \sqrt{\mathbb{E}_{x \sim D_A} [||\nabla_{y(x)} d(y(x)) - (h(x) - y(x))||_2^2]} \tag{42}$$

Since y is measurable, by a change of variables (cf. Varadhan (2002), Thm. 1.9), we have:

$$\begin{aligned}
 \mathbb{E}_{x \sim D_A} [||\nabla_{y(x)} d(y(x)) - (h(x) - y(x))||_2^2] &= \mathbb{E}_{z \sim y \circ D_A} [||\nabla_z d(z) - (h(y^{-1}(z)) - z)||_2^2] \\
 &= \mathbb{E}_{z \sim D_B} [||\nabla_z d(z) - (h(y^{-1}(z)) - z)||_2^2] = R_{D_B}[h \circ y^{-1} - \text{Id}, \nabla d]
 \end{aligned} \tag{43}$$

Therefore, by combining Eqs. 42 and 43, we have:

$$\mathbb{E}_{x \sim D_A} [||\nabla_{y(x)} d(y(x)) - (h(x) - y(x))||_2] \leq \sqrt{R_{D_B}[h \circ y^{-1} - \text{Id}, \nabla d]} \tag{44}$$

Finally, by combining Eqs. 41 and 44 and $\beta(d) < 2$, we obtain the desired inequality. \blacksquare

The following lemma is a variation of the Occam's Razor theorem from Benaim et al. (2018), where it was used to bound the risk between $h_1 \in \mathcal{H}$ and the target function y , when assuming that there is a good approximation for y in, what appears here as \mathcal{P}_ω .

Lemma 6 *Let $y \in \mathcal{T}$ be a target function. Then, for every function $h_1 \in \mathcal{P}_\omega$, we have:*

$$R_{D_A}[h_1, y] \lesssim \sup_{h_2 \in \mathcal{P}_\omega} R_{D_A}[h_1, h_2] + \inf_{h \in \mathcal{P}_\omega} R_{D_A}[h, y] \tag{45}$$

Proof First, we consider that $\ell(a, c) = ||a - c||_2^2 = ||a - b + b - c||_2^2 \leq (||a - b||_2 + ||b - c||_2)^2 = ||a - b||_2^2 + ||b - c||_2^2 + 2||a - b||_2 \cdot ||b - c||_2 \leq ||a - b||_2^2 + ||b - c||_2^2 + 2 \max(||a - b||_2^2, ||b - c||_2^2) \leq 3(||a - b||_2^2 + ||b - c||_2^2) = 3(\ell(a, b) + \ell(b, c))$. Therefore, we have:

$$\begin{aligned}
 R_{D_A}[h_1, y] &= \mathbb{E}_{x \sim D_A} [||h_1(x) - y(x)||_2^2] \\
 &\leq \mathbb{E}_{x \sim D_A} [3 \{||h_1(x) - h^*(x)||_2^2 + ||h^*(x) - y(x)||_2^2\}] \\
 &= 3 \{R_{D_A}[h_1, h^*] + R_{D_A}[h^*, y]\} \\
 &= 3 \left\{ R_{D_A}[h_1, h^*] + \inf_{h \in \mathcal{P}_\omega} R_{D_A}[h, y] \right\}
 \end{aligned} \tag{46}$$

where $h^* \in \arg \inf_{h \in \mathcal{P}_\omega} R_{D_A}[h^*, y]$. Since $h^* \in \mathcal{P}_\omega$, we have: $R_{D_A}[h_1, h^*] \leq \sup_{h_2 \in \mathcal{P}_\omega} R_{D_A}[h_1, h_2]$ and the desired inequality follows immediately. \blacksquare

The following result is obtained by combining Lem. 5 with Lem. 6.

Lemma 7 Assume the settings of Sec. 2.2 and Sec. 4. Let $y \in \mathcal{T}$ be a target function, $\omega \in \Omega$, $h \in \mathcal{P}_\omega$ such that $h : \mathcal{X}_A \rightarrow \mathcal{X}_B$ and $d \in \mathcal{C}$ such that $\beta(d) < 2$. Then, for every function $h_1 \in \mathcal{H}$, we have:

$$\begin{aligned} R_{D_A}[h_1, y] \leq & 3 \sup_{h_2 \in \mathcal{P}_\omega} R_{D_A}[h_1, h_2] + \frac{6\rho_C(h \circ D_A, D_B)}{2 - \beta(d)} \\ & + \frac{6 \sup_{u \in \mathcal{X}_A} \|h(u) - y(u)\|_2}{2 - \beta(d)} \sqrt{R_{D_B}[h \circ y^{-1} - \text{Id}, \nabla d]} \end{aligned} \quad (47)$$

Proof Let $y \in \mathcal{T}$, $\omega \in \Omega$, $h \in \mathcal{P}_\omega$ such that $h : \mathcal{X}_A \rightarrow \mathcal{X}_B$ and $d \in \mathcal{C}$ such that $\beta(d) < 2$. By Lem. 5:

$$R_{D_A}[h, y] \leq \frac{2\rho_C(h \circ D_A, D_B)}{2 - \beta(d)} + \frac{2 \sup_{u \in \mathcal{X}_A} \|h(u) - y(u)\|_2}{2 - \beta(d)} \sqrt{R_{D_B}[h \circ y^{-1} - \text{Id}, \nabla d]} \quad (48)$$

In particular, since $h \in \mathcal{P}_\omega$, we have: $\inf_{h^* \in \mathcal{P}_\omega} R_{D_A}[h^*, y] \leq R_{D_A}[h, y]$. By combining Eq. 11 (of Lem. 6) with Eq. 48, we obtain the desired inequality. \blacksquare

Theorem 2 (Cross-Domain Mapping with IPMs - The Non-Deterministic Case) Assume the settings of Sec. 2.2 and Sec. 4. Let $\omega \in \Omega$, $h \in \mathcal{P}_\omega$ such that $h : \mathcal{X}_A \rightarrow \mathcal{X}_B$ and $d \in \mathcal{C}$ such that $\beta(d) \leq 1$. Then, for every $h_1 \in \mathcal{P}_\omega$, we have:

$$\inf_{y \in \mathcal{T}} R_{D_A}[h_1, y] \lesssim \sup_{h_2 \in \mathcal{P}_\omega} R_{D_A}[h_1, h_2] + \rho_C(h \circ D_A, D_B) + \inf_{y \in \mathcal{T}} \sqrt{R_{D_B}[h \circ y^{-1} - \text{Id}, \nabla d]} \quad (27)$$

Proof Let $\omega \in \Omega$, $h \in \mathcal{P}_\omega$ such that $h : \mathcal{X}_A \rightarrow \mathcal{X}_B$, $d \in \mathcal{C}$ such that is $\beta(d) \leq 1$ and $y \in \mathcal{T}$. Then, by Lem. 7, for every $h_1 \in \mathcal{P}_\omega$, we have:

$$\begin{aligned} R_{D_A}[h_1, y] \leq & 3 \sup_{h_2 \in \mathcal{P}_\omega} R_{D_A}[h_1, h_2] + 6\rho_C(h \circ D_A, D_B) \\ & + 6 \sup_{u \in \mathcal{X}_A} \|h(u) - y(u)\|_2 \sqrt{R_{D_B}[h \circ y^{-1} - \text{Id}, \nabla d]} \end{aligned} \quad (49)$$

In particular, since \mathcal{X}_B is bounded, there is a constant $K > 0$ such that $\sup_{a,b \in \mathcal{X}_B} \|a - b\|_2 \leq K$. Hence, for every $h, y : \mathcal{X}_A \rightarrow \mathcal{X}_B$, we have: $\sup_{u \in \mathcal{X}_A} \|h(u) - y(u)\|_2 \leq K$. Therefore,

$$R_{D_A}[h_1, y] \lesssim \sup_{h_2 \in \mathcal{P}_\omega} R_{D_A}[h_1, h_2] + \rho_C(h \circ D_A, D_B) + \sqrt{R_{D_B}[h \circ y^{-1} - \text{Id}, \nabla d]} \quad (50)$$

Finally, by taking $\inf_{y \in \mathcal{T}}$ in both sides of Eq. 50, we obtain the desired inequality. \blacksquare

Theorem 1 (Cross-Domain Mapping with IPMs) Assume the settings of Sec. 2.2 and Sec. 4. Let $\omega \in \Omega$, $h \in \mathcal{P}_\omega$ such that $h : \mathcal{X}_A \rightarrow \mathcal{X}_B$ and $d \in \mathcal{C}$ such that $\beta(d) \leq 1$. Then, for every $h_1 \in \mathcal{P}_\omega$, we have:

$$R_{D_A}[h_1, y] \lesssim \sup_{h_2 \in \mathcal{P}_\omega} R_{D_A}[h_1, h_2] + \rho_C(h \circ D_A, D_B) + \sqrt{R_{D_B}[h \circ y^{-1} - \text{Id}, \nabla d]} \quad (13)$$

Proof Follows immediately from Thm. 2 for $\mathcal{T} = \{y\}$.

Corollary 8 (Cross-Domain Mapping with WGANs - The Non-Deterministic Case) *Assume the settings of Sec. 2.2 and Sec. 4. In addition, assume that $\mathcal{T} \in C_{\text{diff}}^1$, $\mathcal{H} \subset C^1$ and that for every $\omega \in \Omega$, we have: $\mathcal{P}_\omega \cap \mathcal{Q} \neq \emptyset$. Then, for every $\omega \in \Omega$ and $h_1 \in \mathcal{P}_\omega$, we have:*

$$\inf_{y \in \mathcal{T}} R_{D_A}[h_1, y] \lesssim \sup_{h_2 \in \mathcal{P}_\omega} R_{D_A}[h_1, h_2] + \inf_{h \in \mathcal{P}_\omega \cap \mathcal{Q}} \mathbf{W}(h \circ D_A, D_B) \quad (28)$$

Proof Let $\omega \in \Omega$ and $h_\omega \in \arg \inf_{h \in \mathcal{P}_\omega \cap \mathcal{Q}} \mathbf{W}(h \circ D_A, D_B)$. Since $h_\omega \in \mathcal{Q}$, there is a function $y_\omega \in \mathcal{T}$ such that:

$$\sup_{z \in \mathcal{X}_B} \|\mathcal{J}_{h_\omega \circ y_\omega^{-1} - \text{Id}}(z)\|_2 \leq 1 \quad (51)$$

Since \mathcal{X}_B , there is a constant $K > 0$ such that $\sup_{z \in \mathcal{X}_B} \|z\|_2 \leq K$. We consider that $h_\omega, y_\omega : \mathcal{X}_A \rightarrow \mathcal{X}_B$, and, therefore, for every $z, u \in \mathcal{X}_B$, we have: $h_\omega(y_\omega^{-1}(z)) \in \mathcal{X}_B$. In particular,

$$\sup_{z \in \mathcal{X}_B} \|h_\omega(y_\omega^{-1}(z)) - z\|_2 \leq 2K \quad (52)$$

We select a set of discriminators $\mathcal{C} = \{d : \mathcal{X}_B \rightarrow \mathbb{R} \mid \|d\|_{\text{Lip}} \leq 2K\}$. In addition, since $y_\omega \in C_{\text{diff}}^1$ and $h_\omega \in C^1$, we have: $h_\omega(y_\omega^{-1}(z)) - z \in C^1$ and there is an anti-derivative function d such that:

$$\nabla d(z) = h_\omega(y_\omega^{-1}(z)) - z \quad (53)$$

By Eqs. 52 and 53, $d \in \mathcal{C}$. In addition, $d \in C^2$ since $h_\omega(y_\omega^{-1}(z)) - z \in C^1$. Furthermore, by Eq. 53, $H_d(z) = \mathcal{J}_{h_\omega \circ y_\omega^{-1} - \text{Id}}$ and by Eq. 51, we conclude that $\beta(d) \leq 1$. Therefore, by Lem. 2 and Eq. 53, for any $h_1 \in \mathcal{P}_\omega$, we have:

$$\begin{aligned} \inf_{y \in \mathcal{T}} R_{D_A}[h_1, y] &\lesssim \sup_{h_2 \in \mathcal{P}_\omega} R_{D_A}[h_1, h_2] + \rho_{\mathcal{C}}(h_\omega \circ D_A, D_B) + \sqrt{R_{D_B}[h_\omega \circ y_\omega^{-1} - \text{Id}, \nabla d]} \\ &= \sup_{h_2 \in \mathcal{P}_\omega} R_{D_A}[h_1, h_2] + \rho_{\mathcal{C}}(h_\omega \circ D_A, D_B) \end{aligned} \quad (54)$$

Finally, since $\mathcal{C} = \{d : \mathcal{X}_B \rightarrow \mathbb{R} \mid \|d\|_{\text{Lip}} \leq 2K\}$, for any two distributions D_1 and D_2 , we have: $\rho_{\mathcal{C}}(D_1, D_2) = 2K \cdot \mathbf{W}(D_1, D_2)$ and by the definition of h_ω , we have: $\mathbf{W}(h_\omega \circ D_A, D_B) = \inf_{h \in \mathcal{P}_\omega \cap \mathcal{Q}} \mathbf{W}(h \circ D_A, D_B)$. Therefore,

$$\begin{aligned} \inf_{y \in \mathcal{T}} R_{D_A}[h_1, y] &\lesssim \sup_{h_2 \in \mathcal{P}_\omega} R_{D_A}[h_1, h_2] + 2K \cdot \mathbf{W}(h_\omega \circ D_A, D_B) \\ &= \sup_{h_2 \in \mathcal{P}_\omega} R_{D_A}[h_1, h_2] + 2K \cdot \inf_{h \in \mathcal{P}_\omega \cap \mathcal{Q}} \mathbf{W}(h \circ D_A, D_B) \\ &\lesssim \sup_{h_2 \in \mathcal{P}_\omega} R_{D_A}[h_1, h_2] + \inf_{h \in \mathcal{P}_\omega \cap \mathcal{Q}} \mathbf{W}(h \circ D_A, D_B) \end{aligned} \quad (55)$$

■

Corollary 9 (Cross-Domain Mapping with WGANs) *Assume the settings of Sec. 2.2 and Sec. 4. In addition, assume that $y \in C_{\text{diff}}^1$, $\mathcal{H} \subset C^1$ and that for every $\omega \in \Omega$, we have: $\mathcal{P}_\omega \cap \mathcal{Q} \neq \emptyset$. Then, for every $\omega \in \Omega$ and $h_1 \in \mathcal{P}_\omega$, we have:*

$$R_{D_A}[h_1, y] \lesssim \sup_{h_2 \in \mathcal{P}_\omega} R_{D_A}[h_1, h_2] + \inf_{h \in \mathcal{P}_\omega \cap \mathcal{Q}} \mathbf{W}(h \circ D_A, D_B) \quad (16)$$

Proof Follows immediately from Cor. 4 for $\mathcal{T} = \{y\}$.

Lemma 10 Assume the setting of Sec. 2.2 such that $M = N$. Assume that the sets \mathcal{X}_A and \mathcal{X}_B are convex and open. Let $h, y : \mathcal{X}_A \rightarrow \mathcal{X}_B$ such that $h \in C^1$ and $y \in C_{\text{diff}}^1$. If $\mathcal{J}_{y^{-1}}(z) \neq 0$ for every $z \in \mathcal{X}_B$ and $\|h - y\|_{\text{Lip}} \leq \|y^{-1}\|_{\text{Lip}}^{-1}$, then, $\|h \circ y^{-1} - \text{Id}\|_{\text{Lip}} \leq 1$.

Proof Since $y \in C_{\text{diff}}^1$, $h \in C^1$ and \mathcal{X}_A and \mathcal{X}_B are convex sets, we have: (i) $\|y^{-1}\|_{\text{Lip}} = \sup_{z \in \mathcal{X}_B} \|\mathcal{J}_{y^{-1}}(z)\|_2$, (ii) $\|h - y\|_{\text{Lip}} = \sup_{x \in \mathcal{X}_A} \|\mathcal{J}_h(x) - \mathcal{J}_y(x)\|_2$ and (iii) $\|h \circ y^{-1} - \text{Id}\|_{\text{Lip}} = \sup_{z \in \mathcal{X}_B} \|\mathcal{J}_{h \circ y^{-1} - \text{Id}}(z)\|_2$. We consider that:

$$\begin{aligned} & \sup_{x \in \mathcal{X}_A} \|\mathcal{J}_h(x) - \mathcal{J}_y(x)\|_2 \leq 1 / \sup_{z \in \mathcal{X}_B} \|\mathcal{J}_{y^{-1}}(z)\|_2 \\ \implies & \sup_{x \in \mathcal{X}_A} \|\mathcal{J}_h(x) - \mathcal{J}_y(x)\|_2 \cdot \sup_{z \in \mathcal{X}_B} \|\mathcal{J}_{y^{-1}}(z)\|_2 \leq 1 \\ \implies & \sup_{x \in \mathcal{X}_A} \|(\mathcal{J}_h(x) - \mathcal{J}_y(x)) \cdot \mathcal{J}_{y^{-1}}(y(x))\|_2 \leq 1 \end{aligned} \quad (56)$$

Since \mathcal{X}_A is open, by the inverse function theorem, $\mathcal{J}_{y^{-1}}(y(x)) = \mathcal{J}_y(x)^{-1}$ and by the chain rule, $\mathcal{J}_{h \circ y^{-1}}(y(x)) = \mathcal{J}_h(x) \cdot \mathcal{J}_{y^{-1}}(y(x))$. Therefore,

$$\sup_{x \in \mathcal{X}_A} \|\mathcal{J}_{h \circ y^{-1}}(y(x)) - \text{I}\|_2 \leq 1 \quad (57)$$

where I is the identity matrix. In addition, $\mathcal{J}_{\text{Id}}(y(x)) = \text{I}$, where $\text{Id} : \mathcal{X}_B \rightarrow \mathcal{X}_B$ is the identity function. Thus, by linearity of the Jacobian operator:

$$\sup_{x \in \mathcal{X}_A} \|\mathcal{J}_{h \circ y^{-1} - \text{Id}}(y(x))\|_2 \leq 1 \quad (58)$$

Since $y : \mathcal{X}_A \rightarrow \mathcal{X}_B$ is invertible, we have the desired inequality,

$$\|h \circ y^{-1} - \text{Id}\|_{\text{Lip}} = \sup_{z \in \mathcal{X}_B} \|\mathcal{J}_{h \circ y^{-1} - \text{Id}}(z)\|_2 \leq 1 \quad (59)$$

■

Lemma 11 Let $A = (\mathcal{X}_A, D_A)$ and $B = (\mathcal{X}_B, D_B)$ be two domains and \mathcal{P} a class of functions. In addition, let ℓ be a loss function satisfying the triangle inequality. Then, for any target function y and $h_1 \in \mathcal{P}$, we have:

$$\ell(h_1(x), y(x)) \leq \sup_{h_2 \in \mathcal{P}} \ell(h_1(x), h_2(x)) + \inf_{h \in \mathcal{P}} \ell(h(x), y(x)) \quad (23)$$

Proof Let $h^* = \arg \inf_{h \in \mathcal{P}} \ell(h(x), y(x))$. By the triangle inequality, we have: $\ell(h_1(x), y(x)) \leq \ell(h_1(x), h^*(x)) + \ell(h^*(x), y(x)) \leq \sup_{h_2} \ell(h_1(x), h_2(x)) + \inf_{h \in \mathcal{P}} \ell(h(x), y(x))$. ■

Appendix D. Experiments Results

Table 2: Results for Alg. 4 for different datasets. VGG Similarity is given in the first column. The second column gives the separation value, using the linear classifier. In the third column, we measure the discrepancy of the mapping. The last column provides the distance of h to g , where applicable.

Dataset	f	Complexity	Descriptor similarity	Separation accuracy	Discrepancy	Distance $R_{D_A}[h, g]$
Male to Female	g	$k_1 = 6$	0.267	0.928	0.230	-
	g	$k = 8$	0.280	0.938	0.077	-
	g	$k = 10$	0.106	0.940	0.094	-
	g	$k = 12$	0.089	0.940	0.083	-
	h	$k_2 = 8$	0.316	0.933	0.087	0.054
	h	$k_2 = 10$	0.204	0.937	0.109	0.075
	h	$k_2 = 12$	0.197	0.941	0.127	0.077
Female to Male	g	$k_1 = 6$	0.268	0.848	0.310	-
	g	$k = 8$	0.260	0.848	0.107	-
	g	$k = 10$	0.105	0.870	0.075	-
	g	$k = 12$	0.093	0.857	0.076	-
	h	$k_2 = 8$	0.304	0.878	0.107	0.056
	h	$k_2 = 10$	0.215	0.884	0.082	0.083
	h	$k_2 = 12$	0.214	0.883	0.073	0.082
Blond to Black Hair	g	$k_1 = 6$	0.287	0.925	0.214	-
	g	$k = 8$	0.24	0.922	0.092	-
	g	$k = 10$	0.106	0.917	0.097	-
	g	$k = 12$	0.091	0.922	0.094	-
	h	$k_2 = 8$	0.293	0.926	0.136	0.152
	h	$k_2 = 10$	0.197	0.926	0.225	0.161
	h	$k_2 = 12$	0.199	0.928	0.092	0.161
Black to Blond Hair	g	$k_1 = 6$	0.270	0.941	0.264	-
	g	$k = 8$	0.24	0.911	0.073	-
	g	$k = 10$	0.106	0.916	0.094	-
	g	$k = 12$	0.087	0.915	0.084	-
	h	$k_2 = 8$	0.287	0.938	0.077	0.146
	h	$k_2 = 10$	0.179	0.946	0.165	0.149
	h	$k_2 = 12$	0.180	0.952	0.168	0.152



Figure 2: Results for celebA Male to Female transfer (a) Input (b) The mapping obtained by the GAN loss without additional losses.

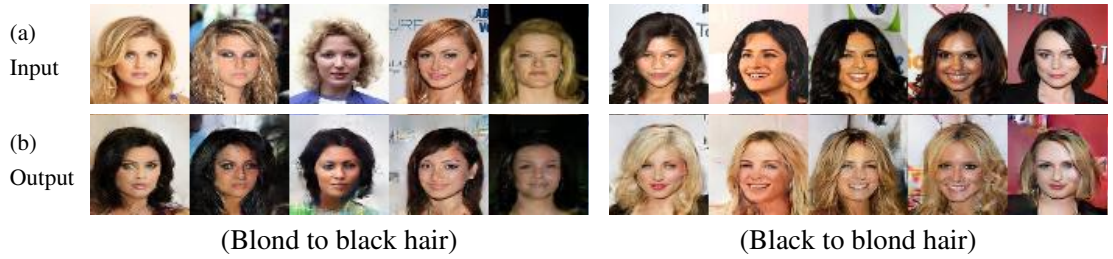


Figure 3: Same as Fig. 2 for black to blond hair conversion.



Figure 4: Same as Fig. 2 for handbag to shoes and shoes to handbag mapping.



Figure 5: Same as Fig. 2 for edges to shoes and shoes to edges conversion.

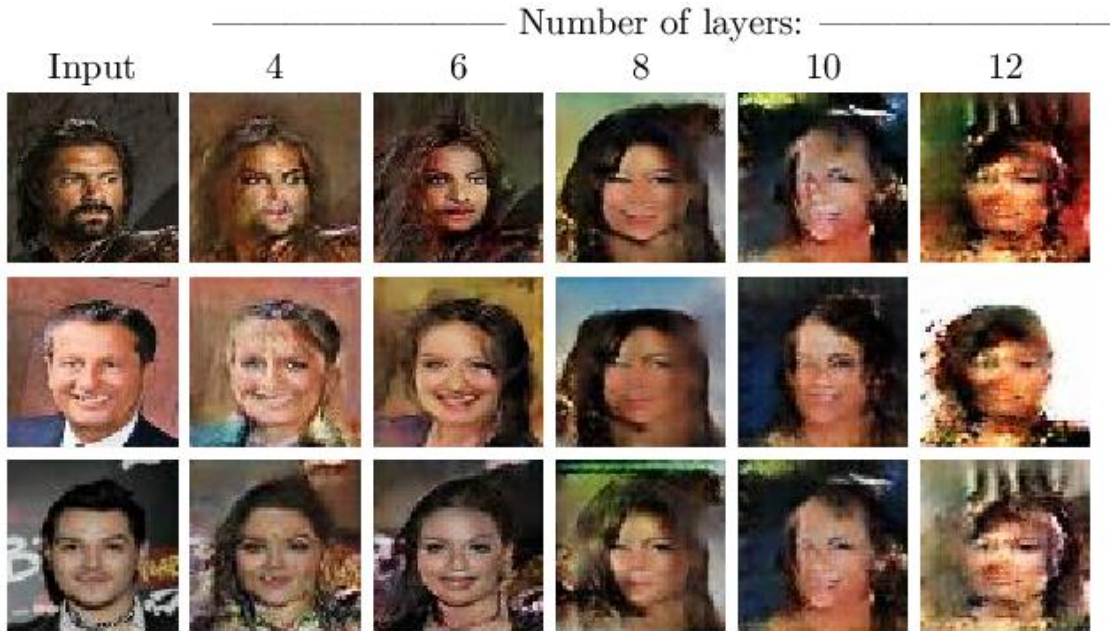


Figure 6: Results for celebA Male to Female transfer for WGAN with varying number of layers.

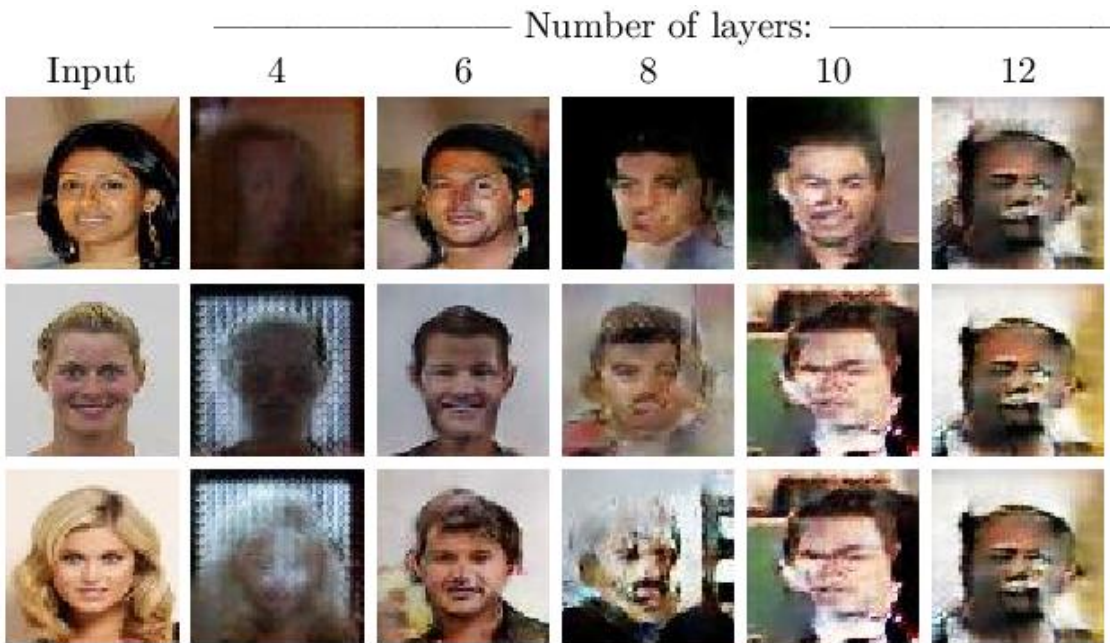


Figure 7: Results for celebA Female to Male transfer for WGAN with varying number of layers.

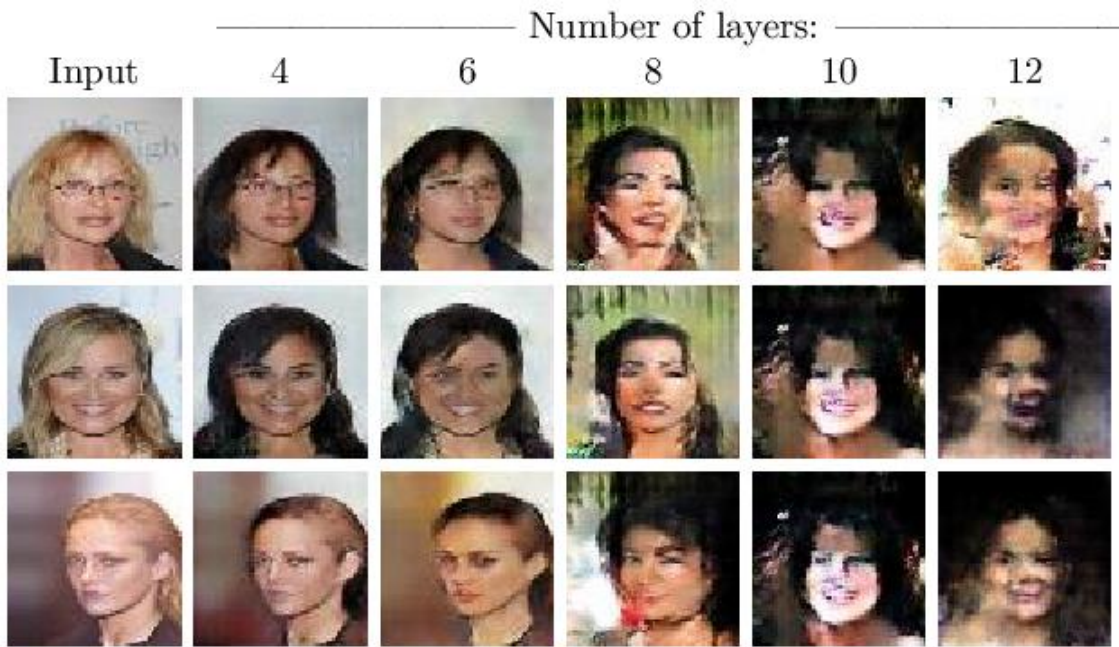


Figure 8: Results for celebA Blond to Black transfer for WGAN with varying number of layers.

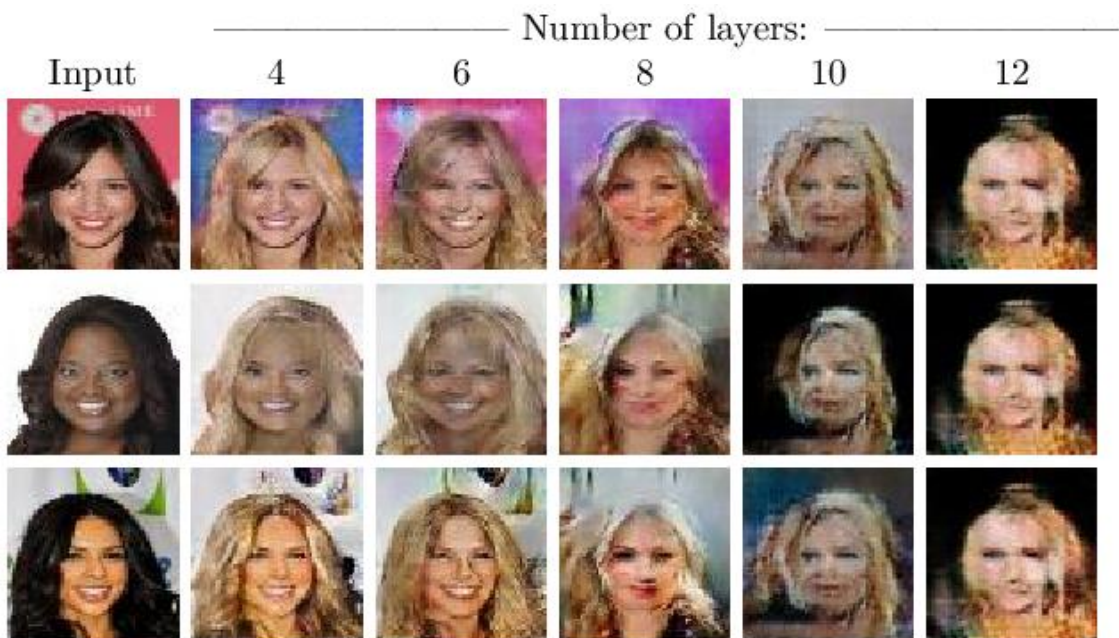


Figure 9: Results for celebA Black to Blond transfer for WGAN with varying number of layers.

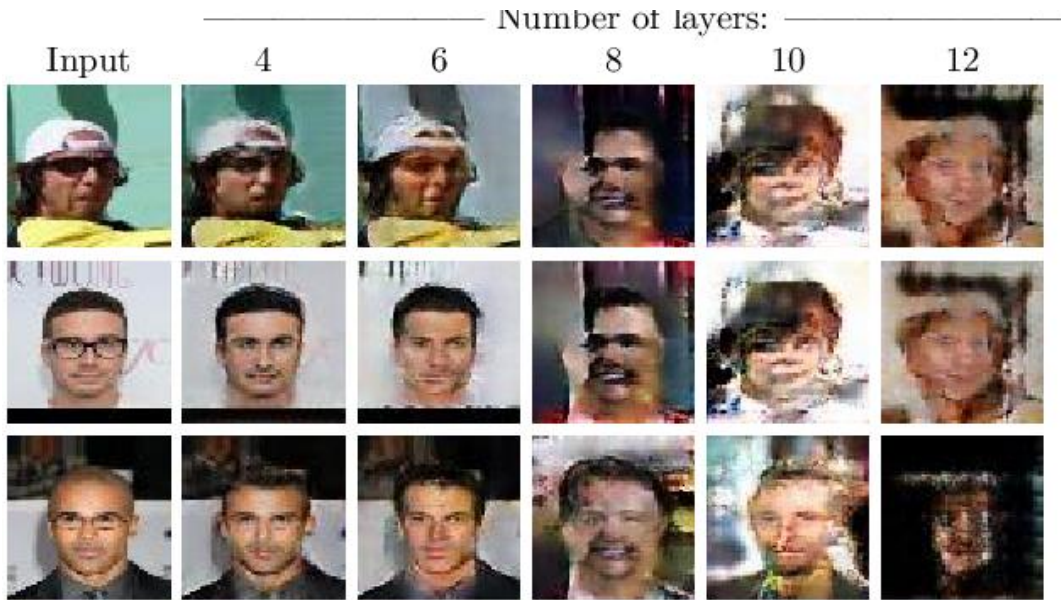


Figure 10: Results for celebA Eyeglasses to Non-Eyeglasses transfer for WGAN with varying number of layers.

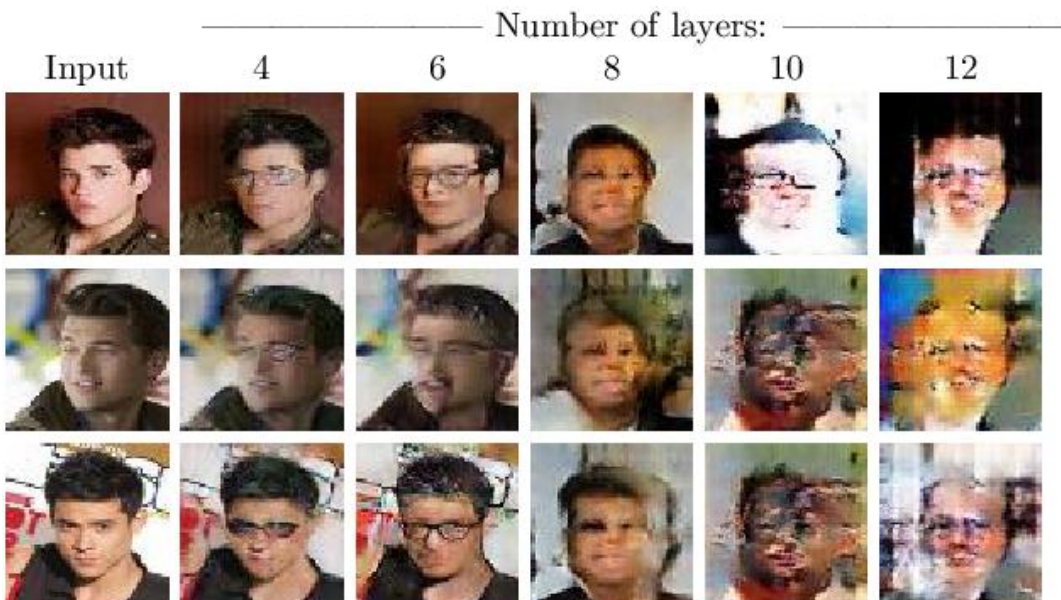


Figure 11: Results for celebA Non-Eyeglasses to Eyeglasses transfer for WGAN with varying number of layers.

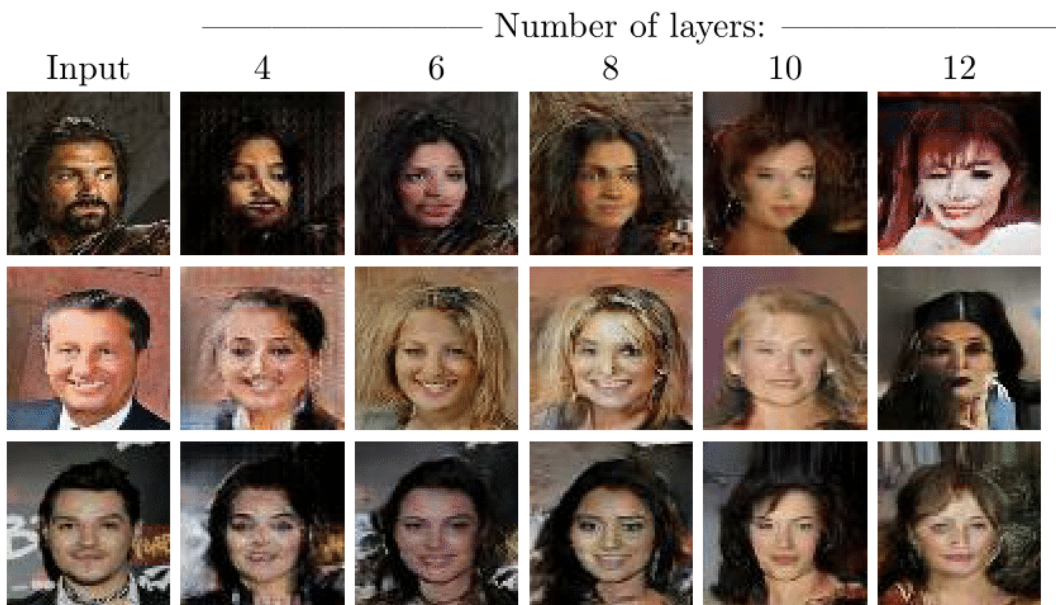


Figure 12: Results for celebA Male to Female transfer for DiscoGAN with varying number of layers.

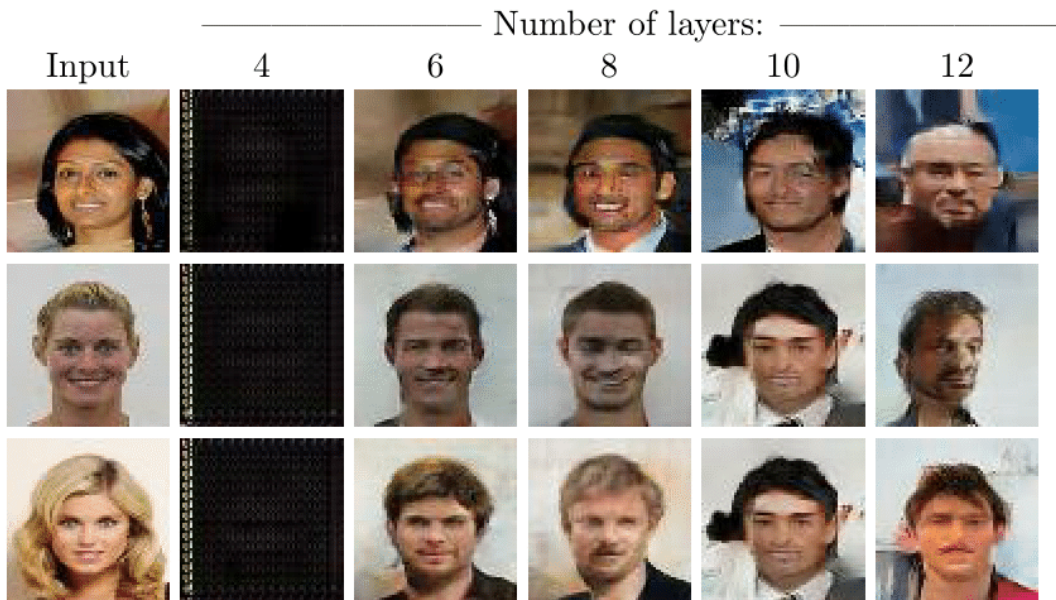


Figure 13: Results for celebA Female to Male transfer for DiscoGAN with varying number of layers.
The case of 4 layers failed to produce acceptable results.

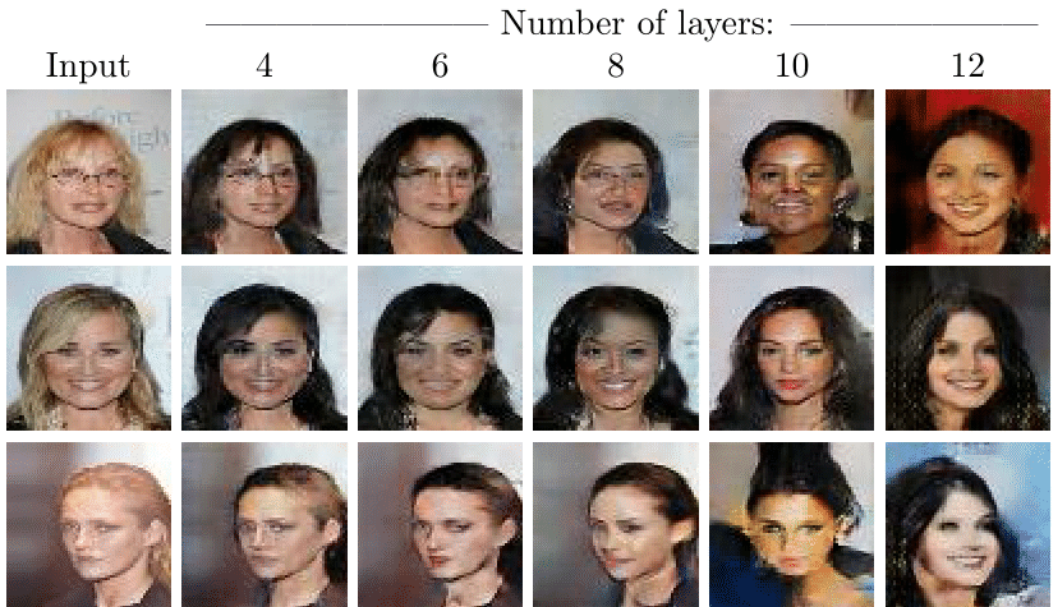


Figure 14: Results for celebA Blond to Black Hair transfer for DiscoGAN with varying number of layers.

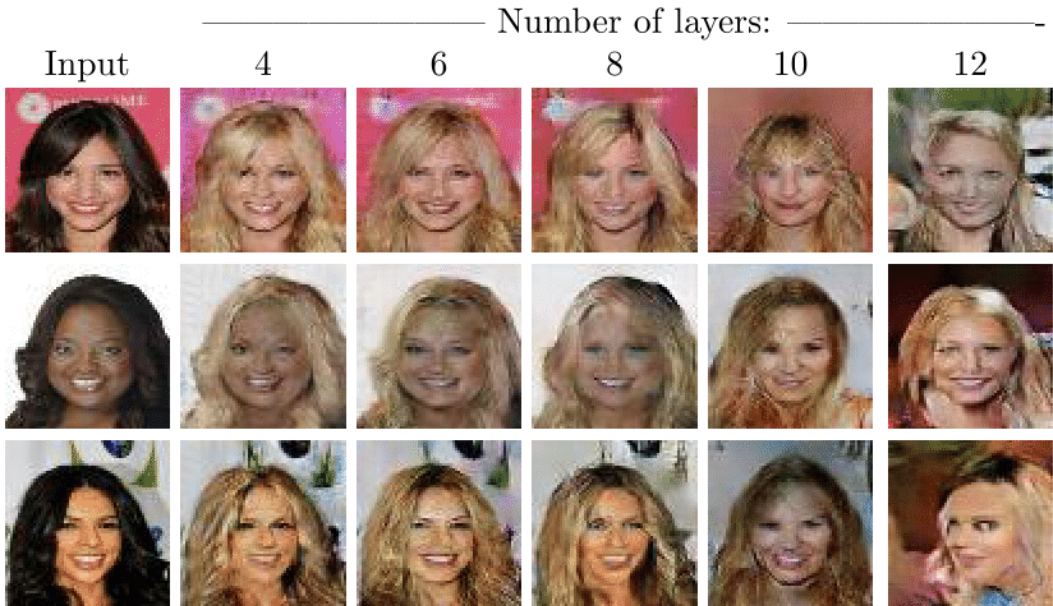


Figure 15: Results for celebA Black Hair to Blond transfer for DiscoGAN with varying number of layers.

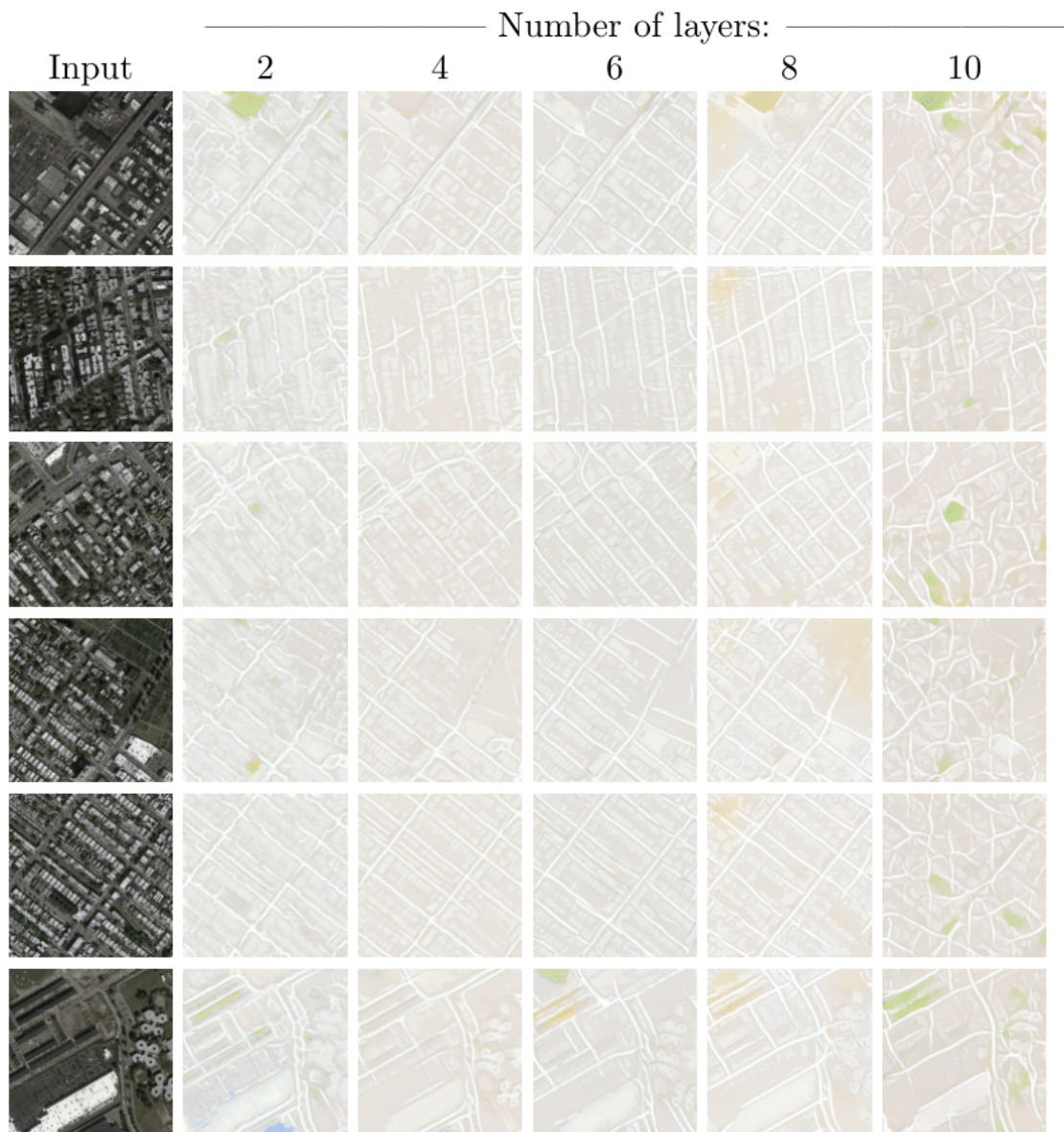


Figure 16: Results for Aerial View Images to Maps transfer for CycleGAN with varying number of layers.

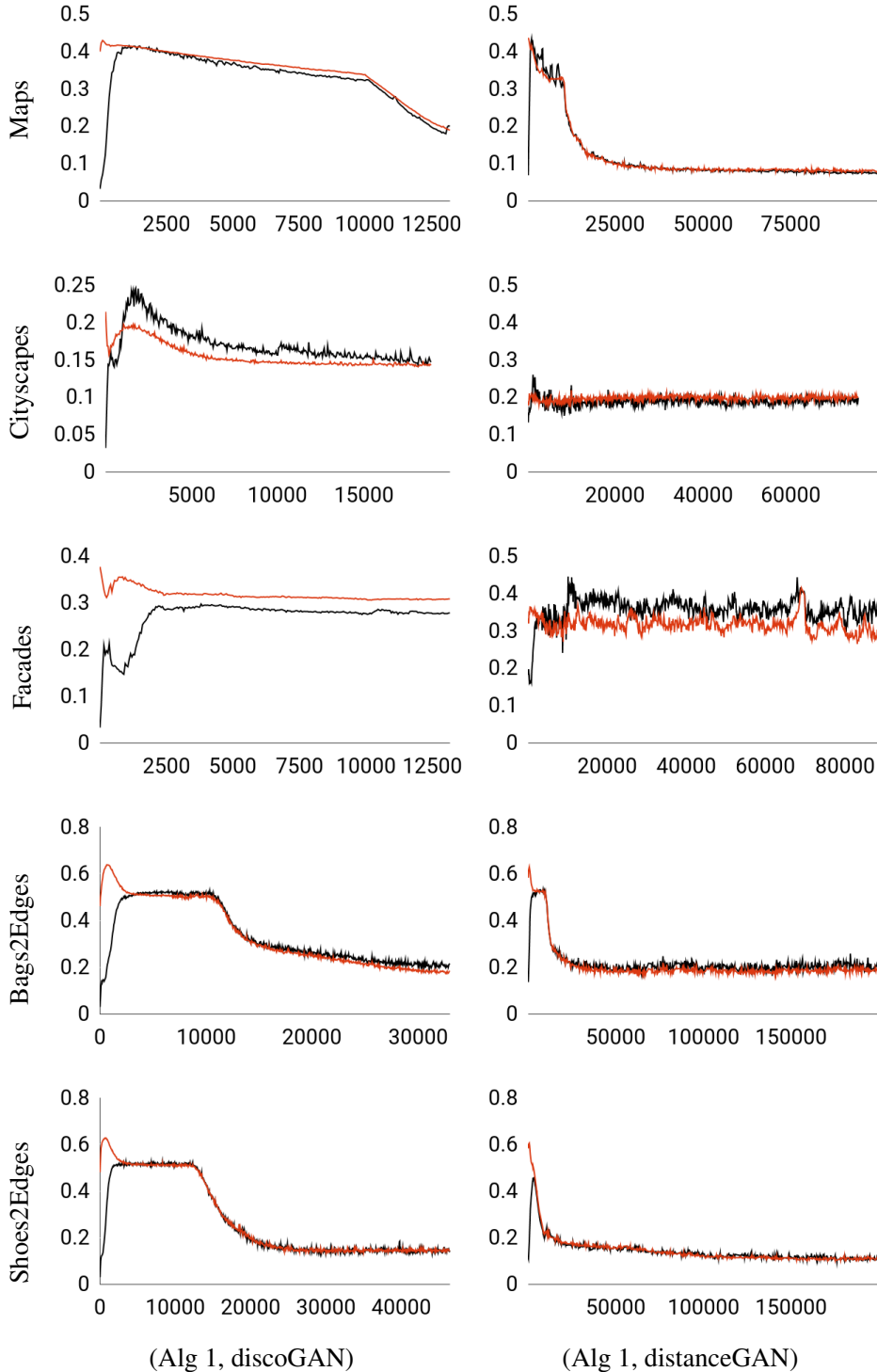


Figure 17: Results of Alg. 1. Ground truth errors are in red and bound in black. x-axis is the iteration or number of layers. y-axis is expected risk. It takes a few epochs for h_1 to have a small enough discrepancy, until which the bound is ineffective.

Table 3: Pearson correlations and the corresponding p-values (in parentheses) of the ground truth error with: (i) the bound, (ii) the GAN losses, and (iii) the circularity losses or (iv) the distance correlation loss. *The cycle loss $A \rightarrow B \rightarrow A$ is shown for DiscoGAN and the distance correlation loss is shown for DistanceGAN.

Alg.	Method	Dataset	Bound	GAN_A	GAN_B	$Cycle_A/L_D^*$	$Cycle_B$
Alg. 1	Disco-GAN Kim et al. (2017)	Shoes2Edges	1.00 (<1E-16)	-0.15 (3E-03)	-0.28 (1E-08)	0.76(<1E-16)	0.79(<1E-16)
		Bags2Edges	1.00 (<1E-16)	-0.26 (6E-11)	-0.57 (<1E-16)	0.85 (<1E-16)	0.84 (<1E-16)
		Cityscapes	0.94 (<1E-16)	-0.66 (<1E-16)	-0.69 (<1E-16)	-0.26 (1E-07)	0.80 (<1E-16)
		Facades	0.85 (<1E-16)	-0.46 (<1E-16)	0.66 (<1E-16)	0.92 (<1E-16)	0.66 (<1E-16)
		Maps	1.00 (<1E-16)	-0.81 (<1E-16)	0.58 (<1E-16)	0.20 (9E-05)	-0.14 (5E-03)
	Distance-GAN Benaim and Wolf (2017)	Shoes2Edges	0.98 (<1E-16)	-	-0.25 (2E-16)	-0.14 (1E-05)	-
		Bags2Edges	0.93 (<1E-16)	-	-0.08 (2E-02)	0.34 (<1E-16)	-
		Cityscapes	0.59 (<1E-16)	-	0.22 (1E-11)	-0.41 (<1E-16)	-
		Facades	0.48 (<1E-16)	-	0.03 (5E-01)	-0.01 (9E-01)	-
		Maps	1.00 (<1E-16)	-	-0.73 (<1E-16)	0.39 (4E-16)	-
Alg. 3	Disco-GAN Kim et al. (2017)	Shoes2Edges	0.92 (<1E-16)	-0.12 (5E-01)	0.02 (9E-01)	0.29 (6E-02)	0.15 (4E-01)
		Bags2Edges	0.96 (<1E-16)	0.25 (1E-01)	0.08 (6E-01)	0.08 (6E-01)	0.05 (7E-01)
		Cityscapes	0.78 (4E-04)	0.24 (4E-01)	-0.16 (6E-01)	-0.04 (9E-01)	0.03 (9E-01)
		Facades	0.80 (6E-10)	0.13 (4E-01)	0.16 (3E-01)	0.20 (2E-01)	0.09 (5E-01)
		Maps	0.66 (1E-03)	0.08 (7E-01)	0.12 (6E-01)	0.17 (5E-01)	-0.25 (3E-01)
	Distance-GAN Benaim and Wolf (2017)	Shoes2Edges	0.98 (<1E-16)	-	-0.05 (7E-01)	0.84 (<1E-16)	-
		Bags2Edges	0.92 (<1E-16)	-	-0.28 (2E-01)	0.45 (3E-02)	-
		Cityscapes	0.51 (4E-04)	-	0.10 (5E-01)	0.28 (2E-2)	-
		Facades	0.72 (<1E-16)	-	-0.01 (1E00)	0.08 (6E-01)	-
		Maps	0.94 (1E-06)	-	0.20 (2E-01)	0.30 (6E-02)	-

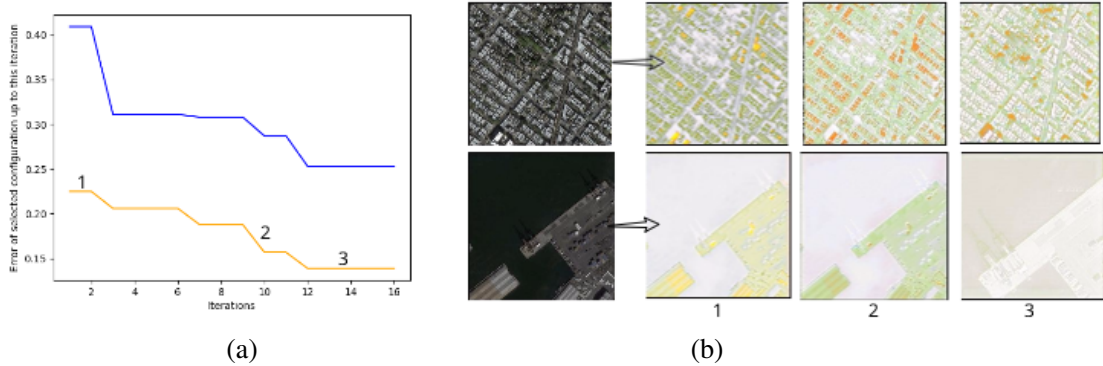


Figure 18: Applying unsupervised hyperband for selecting the best configuration for UNIT for the Maps dataset. (a) blue and orange lines are bound and ground truth error as in Fig. 19. (b) Images produced for three different configurations as indicated on the plot in (a).

IV MAPPING WITH WGANS

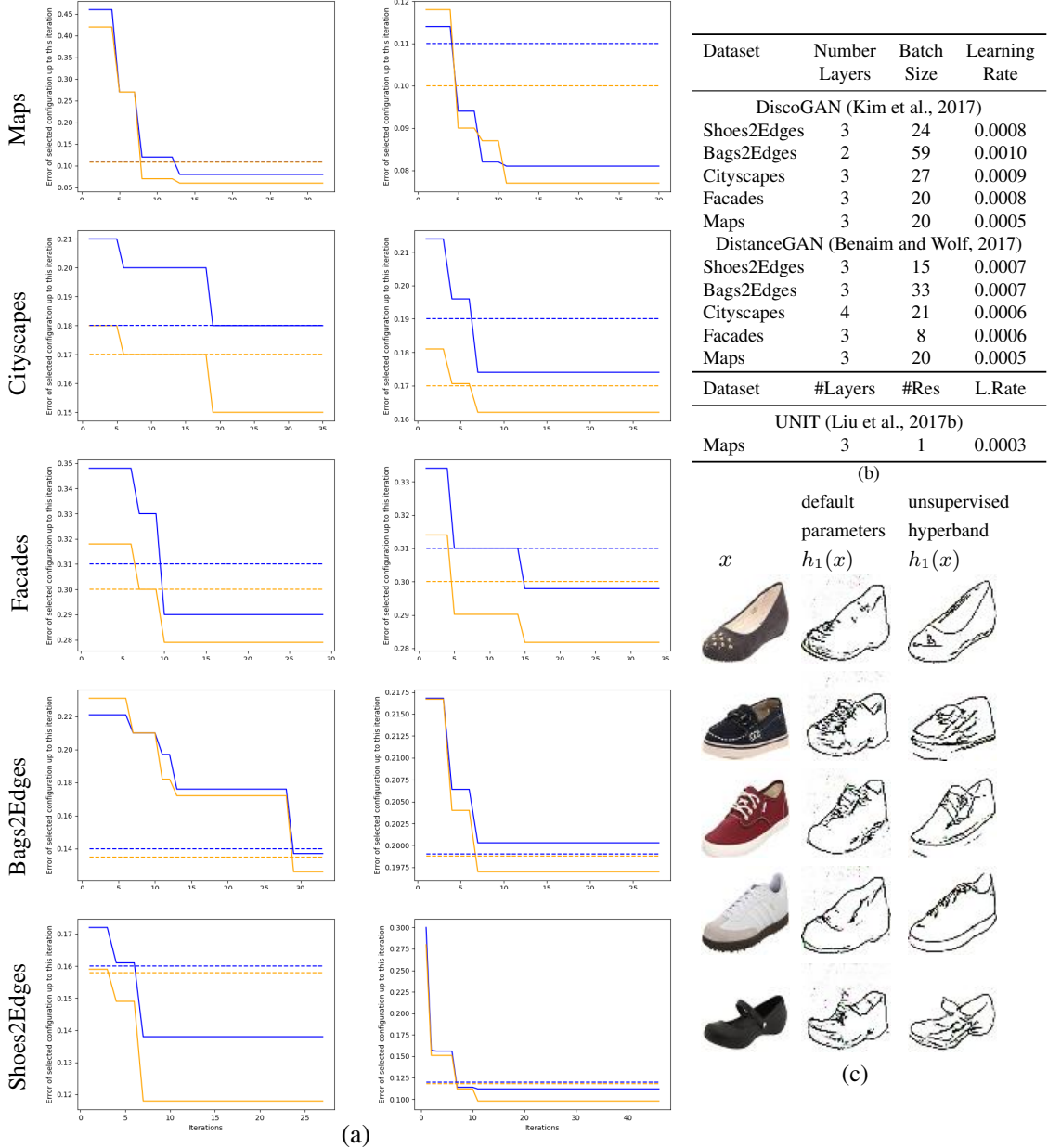


Figure 19: Applying unsupervised hyperband for selecting the best configuration. For DiscoGAN and DistanceGAN, we optimize of the number of encoder and decoder layers, batch size and learning rate, while for UNIT, we optimized for the number of encoder and decoder layers, number of resnet layers and learning rate. (a) For each dataset, the first plot is of DiscoGAN and the second is of DistanceGAN. Hyperband optimizes, according to the bound values indicated in blue. The corresponding ground truth errors are shown in orange. Dotted lines represent the best configuration errors, when varying only the number of layers without hyperband (blue for bound and orange for ground truth error). Each graph shows the error of the best configuration selected by hyperband, as a function the number of hyperband iterations. (b) The corresponding hyperparameters of the best configuration as selected by hyperband. (c) Images produced for DiscoGAN’s shoes2edges: 1st column is the input, the 2nd is the result of DiscoGAN’s default configuration, 3rd is the result of the configuration selected by our unsupervised Hyperband.

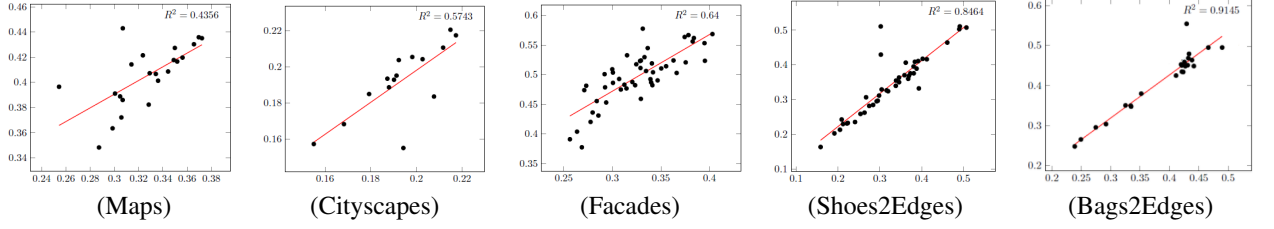


Figure 20: Results of Alg. 3. Results shown for DiscoGAN. The ground truth errors (x-axis) vs. bound (y-axis) are shown per point. The coefficient of determination is shown (top right).

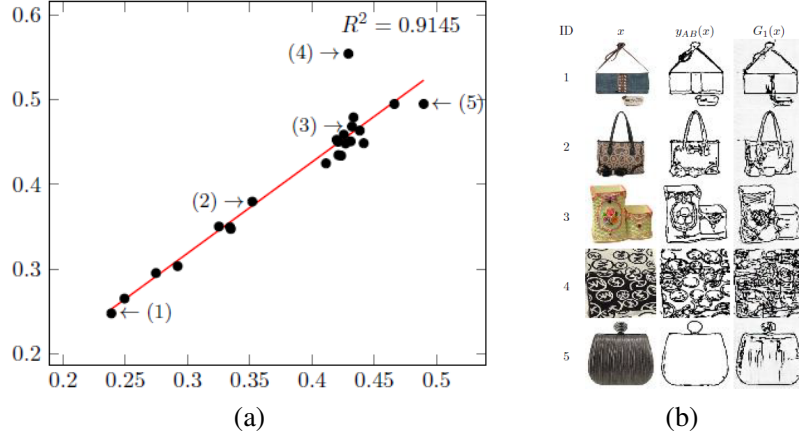


Figure 21: Results of Alg. 3 on DiscoGAN Handbags2Edges. (a) The ground truth errors vs. the bound per point are shown. This is the same as Fig. 23 top right plot with added information identifying specific points. (b) The source (x), ground truth ($y_{AB}(x)$) and mapping ($G_1(x)$) of the marked points.

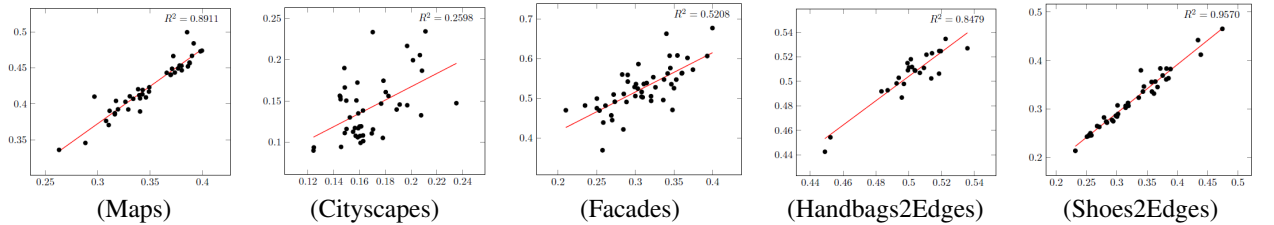


Figure 22: Results of Alg. 3 for DistanceGAN. The ground truth errors (x-axis) vs. the bound (y-axis) are shown per point.

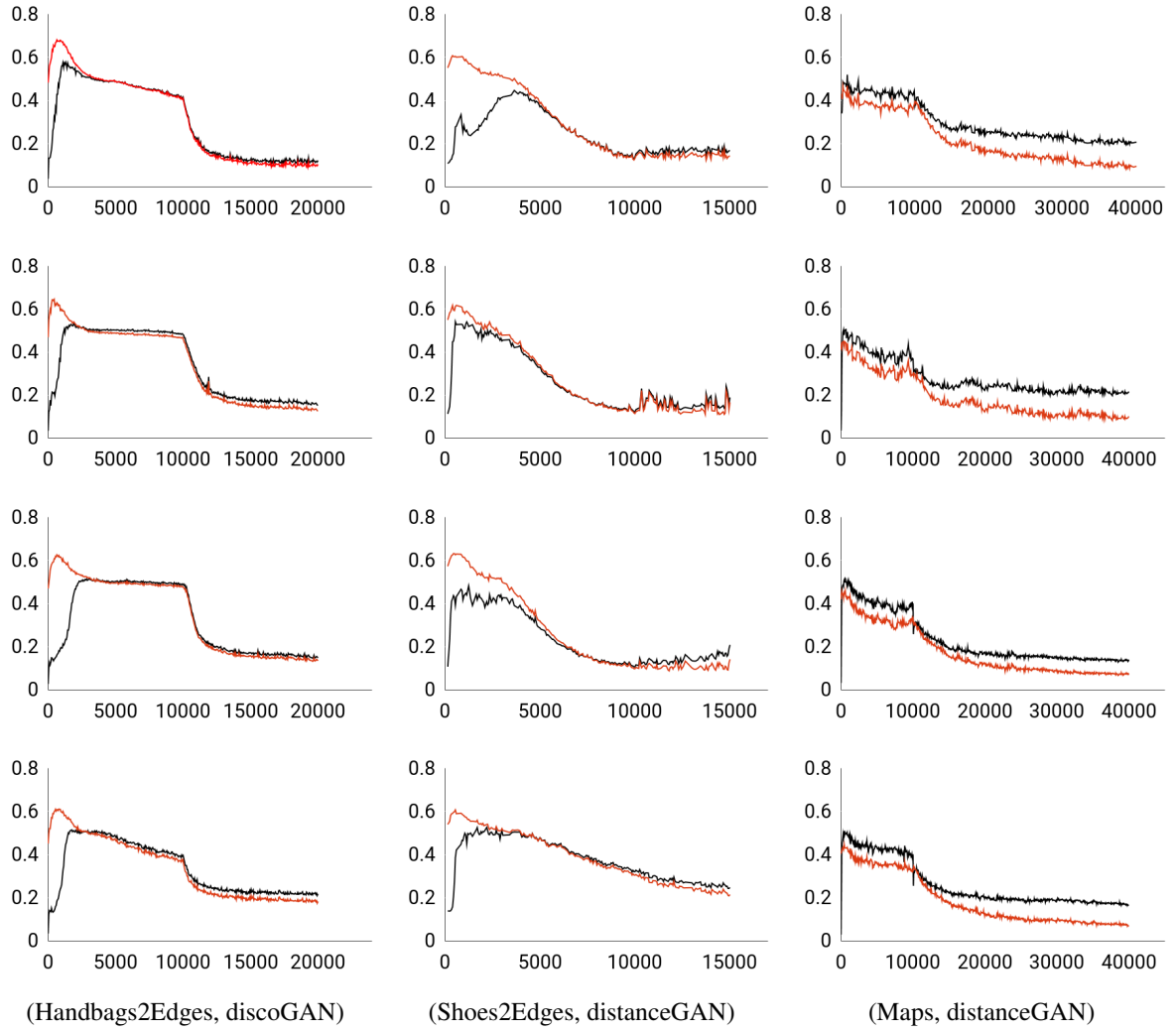


Figure 23: Per-epoch per-sample results for three experiments, four points each. x-axis is iteration. y-axis is the per-sample error. Red line indicates the ground truth error of an individual sample, i.e $\|G_1(x) - y(x)\|_1$. Black line indicates our bound for an individual sample, i.e $\|G_1(x) - G_2(x)\|_1$. Note that it takes a few epochs for G_1 to have a small enough discrepancy, until which the bound is ineffective.

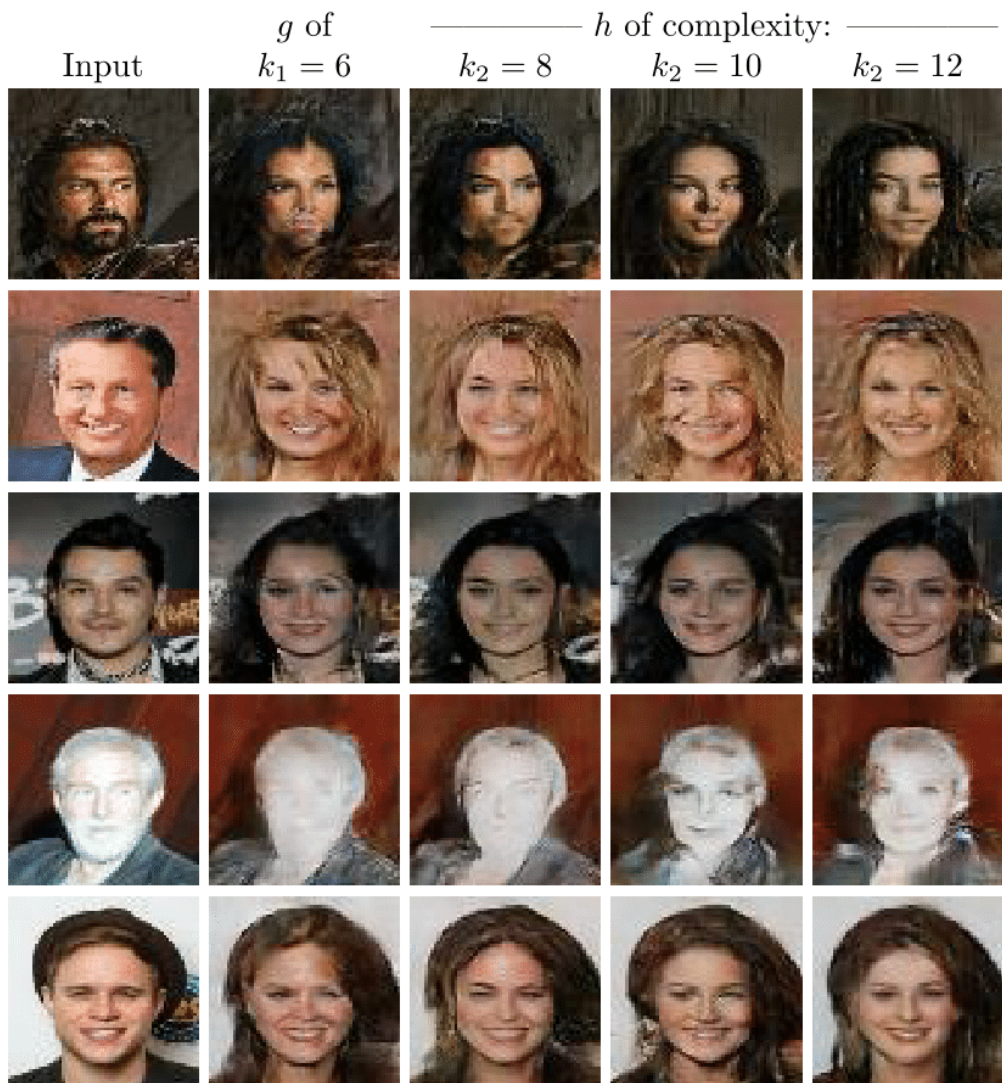


Figure 24: Results for Alg. 4 on Male2Female dataset for mapping Male to Female. Shown is a minimal complexity mapping g that has low discrepancy, and various mappings h obtained by the method.

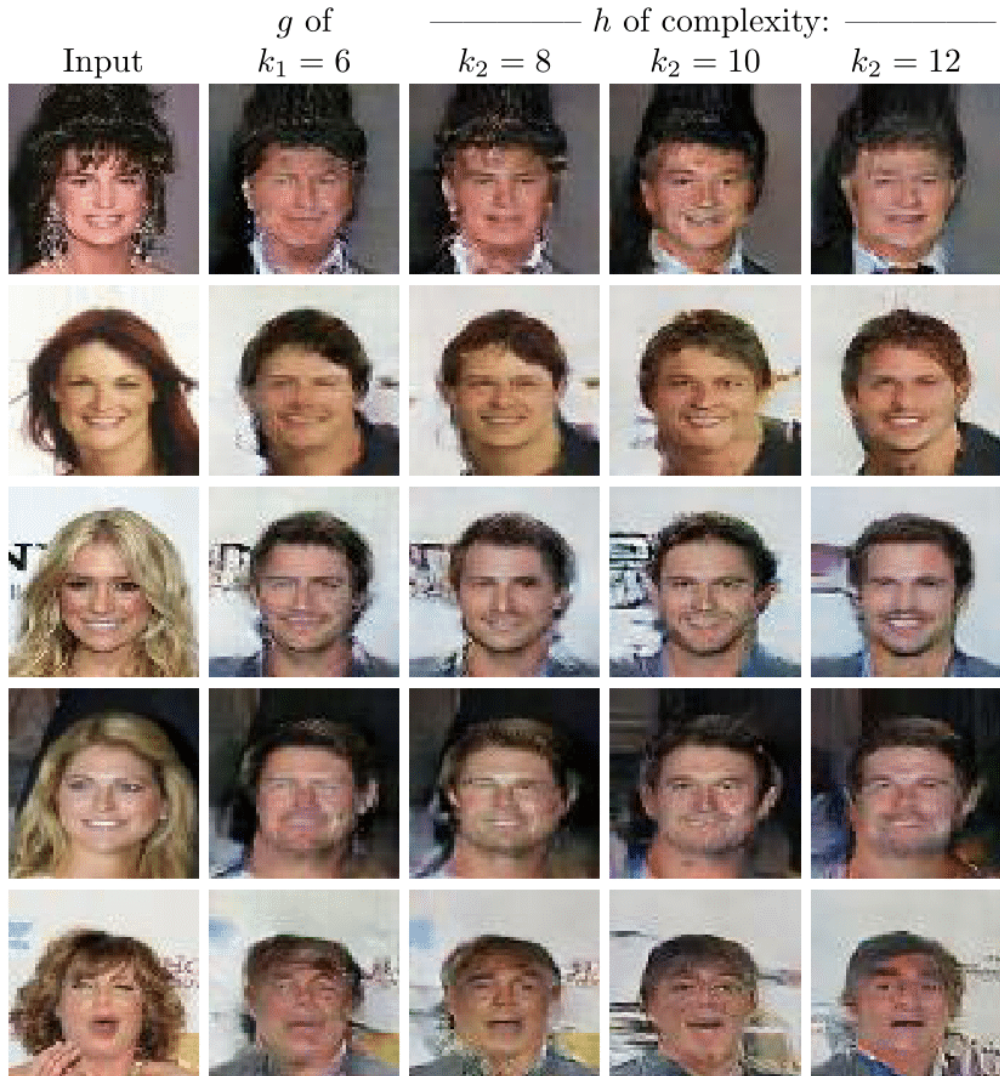


Figure 25: Results for Alg. 4 on Male2Female dataset for mapping Female to Male. Shown is a minimal complexity mapping g that has low discrepancy, and various mappings h obtained by the method.

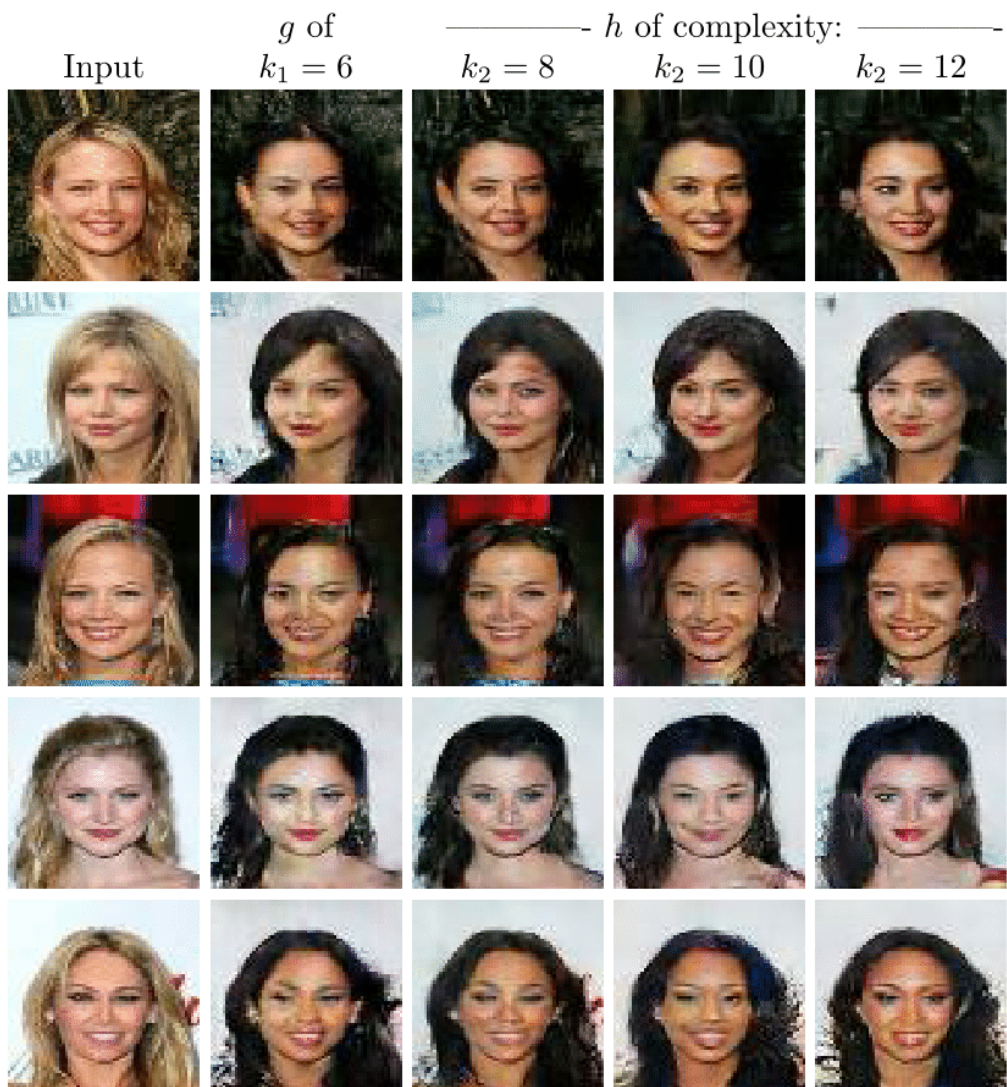


Figure 26: Results for Alg. 4 on celebA dataset for mapping Blond to Black. Shown is a minimal complexity mapping g that has low discrepancy, and various mappings h obtained by the method.



Figure 27: Results for Alg. 4 on celebA dataset for mapping Black to Blond. Shown is a minimal complexity mapping g that has low discrepancy, and various mappings h obtained by the method.



Figure 28: Results for Alg. 4 on Edges2Handbags dataset for mapping Edges to Handbags. Shown is a minimal complexity mapping g that has low discrepancy, and various mappings h obtained by the method.



Figure 29: Results for Alg. 4 on Edges2Shoes dataset for mapping Edges to Shoes. Shown are a minimal complexity mapping g that has low discrepancy, and various mappings h obtained by the method.

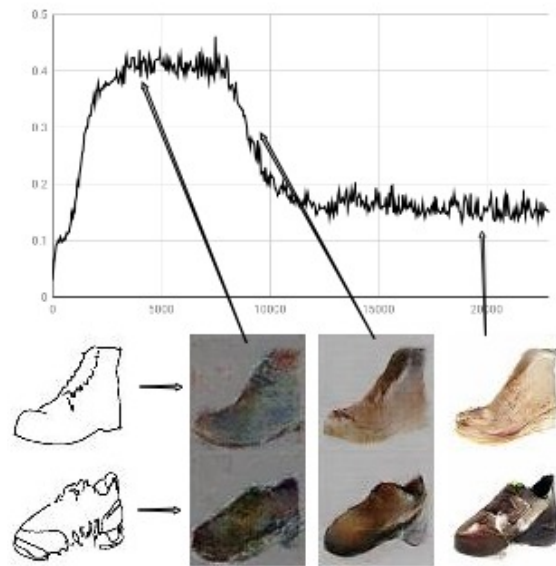


Figure 30: Results for Alg. 5 for non-unique translation of Edges to Shoes. The black line is the bound, images are shown for different bound values.

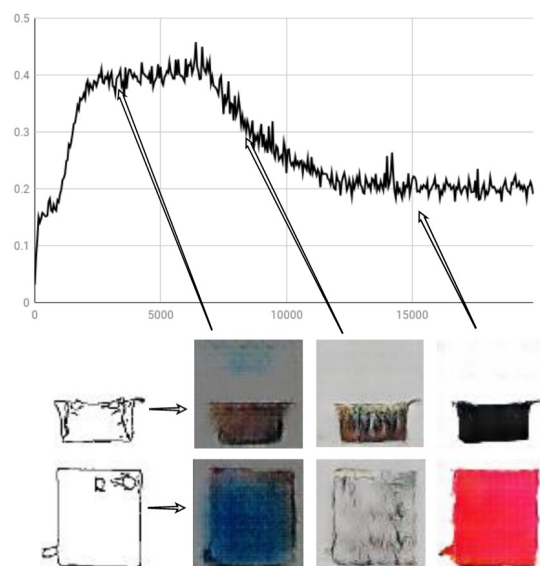


Figure 31: Results for Alg. 5 for non-unique translation of Edges to Handbags. The black line is the bound, images are shown for different bound values.